nature communications

Perspective

https://doi.org/10.1038/s41467-026-73809-3

Climatic reach of small-scale turbulence in the ocean interior

Received: 24 February 2025

Accepted: 20 May 2026

Published online: 09 July 2026

Check for updates

Laura Cimoli[1,18], Ali Mashayek[2,18], Alberto C. Naveira Garabato[3], Colm-cille P. Caulfield[1], Matthew H. Alford[4], Lois Baker[5], B. B. Cael[6], Bieito Fernández Castro[3], Casimir de Lavergne[7], Elizabeth Ellison[8], Geoffrey Gebbie[9], Jonathan Gula[10], Patrick Heimbach[11], Joshua Lanham[1], Arnaud Le Boyer[4], Kate Oglethorpe[2], W. Richard Peltier[12], Helen R. Pillar[11], Alexander M. Piotrowski[2], Sarah G. Purkey[4], Nick Reynard[2], Emily Shuckburgh[13], Martin J. Siegert[14], Alessandro Silvano[3], Luke C. Skinner[2], Carl P. Spingys[15], Lynne D. Talley[4], John R. Taylor[1], Gunnar Voet[4], Richard G. Williams[16], Chris Wilson[17] & Bethan L. Wynne-Cattanach[1]

Small-scale turbulent mixing in the ocean interior is vital in governing ocean circulation and tracer distributions, and hence global climate. However, the planetary extent of this role and its dependence on the microphysics of mixing remain inadequately understood. Here, we emphasize the variety of spatio-temporal scales on which such interior turbulent mixing can shape the climate system. In addition to its well-established role in facilitating the equilibration of deep branches of ocean circulation on centennial-to-millennial timescales, interior turbulent mixing is a leading determinant of oceanic tracer budgets on timescales as short as sub-annual. We highlight the importance of the co-dependence of vertical (diapycnal) mixing and lateral (isopycnal) stirring in establishing the large-scale impacts of oceanic turbulence. We conclude with a summary of theoretical, observational and computational bottlenecks in the way of a sufficiently accurate representation of mixing in Earth System Models, and discuss emerging opportunities for making progress in these areas.

Oceanic tracers are scalar properties that follow the flow and manifest processes and dynamical changes in the ocean system. Tracers can be 'physical' or 'dynamic' (as gradients can lead to buoyancy forces), such as temperature and salinity, or 'bio/geochemical', such as carbon, oxygen and nutrients; 'ventilation' tracers, such as radiocarbon and chlorofluorocarbons, are used for dating seawater, namely determining the length of time since the water was last at the sea surface. Tracers can affect the climate system directly (e.g., heat and carbon) or indirectly (e.g., via changes in primary productivity due to variable nutrient supply). They are transferred by the background flow (advected), drawn into narrow filaments by variations in advection (stirred), and irreversibly transferred to reduce variability (i.e., 'mixed', an intuitive concept of homogenization of scalar fields which we will define more precisely below), which is ultimately achieved by molecular diffusion[1]. This perspective focuses on the last of these processes: the irreversible mixing of tracers driven by small-scale ocean turbulence in the ocean interior.

Small-scale ocean turbulence regulates the global ocean overturning circulation and the distribution of climatically important tracers from the ocean surface to the seafloor, through mechanisms operating on timescales that range from sub-annual to millennial[2–5]. The small spatial scales of three-dimensional turbulence, $\mathcal{O}(10^{-3}-10^{2})$ m, and its spatio-temporal intermittency make it challenging to obtain sufficient samples to quantify turbulent fluxes of water and

A full list of affiliations appears at the end of the paper. e-mail: lc929@cam.ac.uk

tracers accurately, particularly at depth in the ocean water column. Furthermore, turbulence occurs at scales much smaller than the discretized grid cells of Earth System Models (ESMs) and thus must be parameterized. Connecting such microphysics to regional and global physical and biogeochemical processes with horizontal scales of $\mathcal{O}(10^6 - 10^7)$ m remains a monumental challenge[6–9], analogous to the problem of capturing the global climatic implications of cloud microphysics[10].

This perspective is structured as follows. We start with a theoretical definition (and its caveats) of small-scale ocean turbulence, and present canonical observational and modeling efforts. We then showcase the multi-scale role that mixing plays in the climate system, with an emphasis on the short-timescale impacts on tracer budgets. We conclude by discussing ways to overcome several theoretical, observational and computational bottlenecks that limit our understanding and accurate representation of mixing in ESMs.

Defining, observing, and modeling small-scale ocean turbulence

Defining ocean turbulence and mixing

The ocean interior is stably stratified in density, with the densest waters lying deepest. Small-scale stratified turbulence is generated when an energy source is sufficiently strong to overcome the stable background density stratification. Such turbulence inevitably will act to 'mix' the fluid for two related reasons. In this article, we define 'mixing' as the irreversible local homogenization of a spatially varying scalar distribution via molecular diffusion. First, turbulence will tend to increase local scalar gradients at least initially, thus enhancing the diffusive flux. Second, turbulence also tends to increase the surface area of isoscalar levels, thus increasing the total transport of the diffusive flux. Particularly in geophysically relevant flows in the ocean and the atmosphere, this mixing concept in terms of diffusive homogenization of scalar fields can be related to exchanges between energy reservoirs, as irreversible mixing of a statically stable dynamic scalar density field will inevitably lead to an increase in an appropriate 'background potential energy'[11–14]. However, it is always important to remember that 'mixing' homogenizes scalar distributions, and so (of course) 'passive' scalars, such as carbon dioxide, can also be mixed by turbulence. In this case, there is no energetic description in terms of transfers between kinetic and potential energy reservoirs, but there is an irreversible local homogenization of the relevant scalar distribution, justifying why we define that process as 'mixing'.

The processes that underpin cross-density mixing in the ocean interior include the breaking of surface-generated (by winds and/or density gradients) or topographically-induced (by tides or eddy/current-seafloor interactions) internal waves, boundary layer turbulence (such as gravity currents/overflows at high latitudes, and deep canyon mixing), double diffusion (e.g., in the Arctic Ocean), deep convection (e.g. in the Nordic Seas), wake turbulence due to flow around topographic features, and interior vortices (e.g submesoscale coherent vortices)[4,5,15–21] (Fig. 1). This paper focuses on shear-driven diapycnal mixing in the ocean interior and near-bottom boundaries, and does not discuss diffusive mixing (e.g. double diffusion, salt fingering), contributions to mixing due to nonlinearilities of equation of state of seawater, deep convection, or mixed layer dynamics,. The stratification is much stronger below the mixed layer, requiring more energy to mix vertically. It follows that turbulence in the ocean interior is generally weaker and more spatially intermittent than in the surface ocean. As a result, many climate-scale models use overly simplistic or constant 'background' vertical diffusion coefficients in the ocean interior. Here, we highlight the role of small-scale interior turbulence in modulating several dynamical and biogeochemical ocean processes, for which the lack of appropriate parameterizations in climate-scale models poses significant biases.

To illustrate the effect of interior mixing on modulating ocean properties (and the challenges in observing it), Fig. 2 shows the mixing of cold and nutrient-rich Antarctic bottom waters on their northward path through the deep Samoan Passage with the overlying warmer

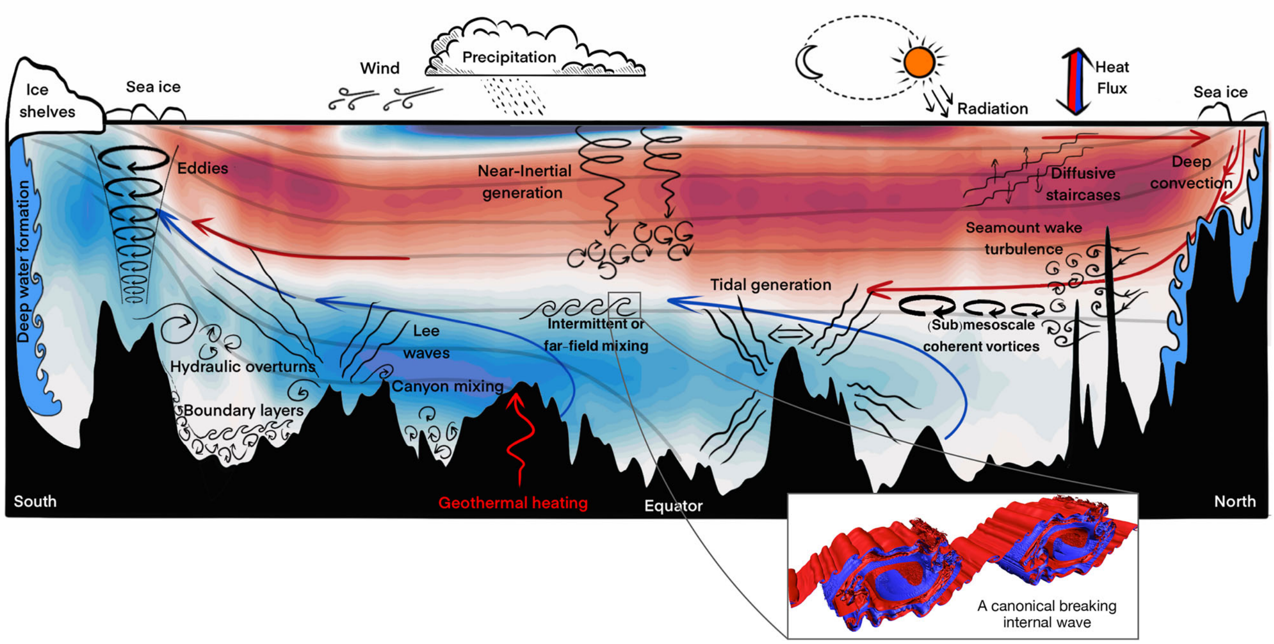

Fig. 1 | Turbulent mixing is ubiquitous at all depths and diverse in nature. The contours (color) in the background show the zonally integrated Meridional Overturning Circulation (MOC), comprising two shallow (less than 500 m deep) subtropical gyres, a clockwise (red) upper cell, and a counterclockwise (blue) lower cell, diagnosed from the Estimating the Circulation and Climate of the Ocean (ECCO) data-assimilating state estimate[133,134]. Thin gray lines represent zonally averaged density surfaces. The MOC is overlaid by a schematic summary of some of the processes that drive the circulation at the surface and bottom, and the processes that induce turbulent mixing in the ocean interior. The bathymetry denotes the ocean seafloor and is representative of the hydrographic sections A16 and A23 in the Atlantic Ocean[51]. The inset shows the transition of a canonical internal wave to turbulence (adapted from Mashayek & Peltier, 2013[135]).

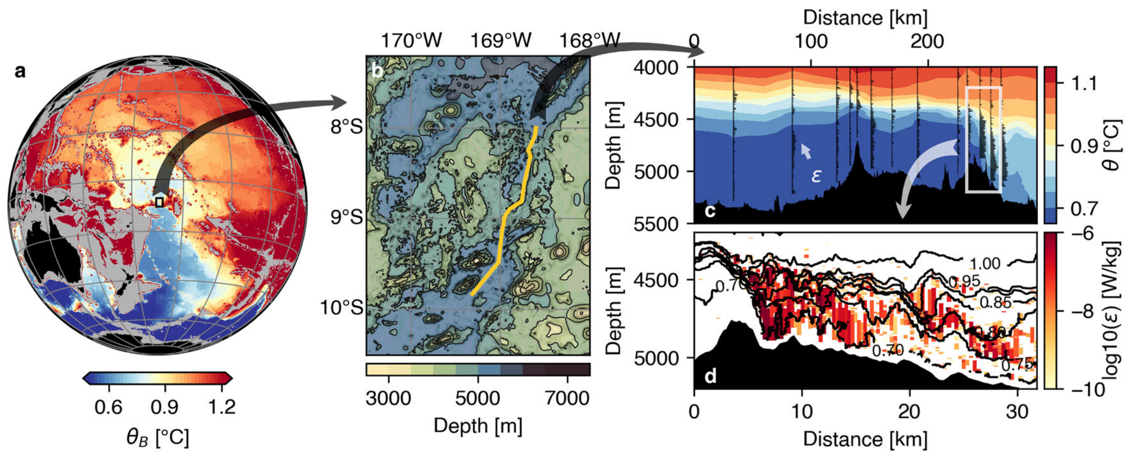

Fig. 2 | Turbulence spans a wide range of scales and is difficult to observe in the deep ocean. a Temperature climatology[50] at the seafloor reveals the northward flow of Antarctic-sourced abyssal waters. As they cross the Samoan Passage (black rectangle), a choke point for the Pacific Overturning Circulation, they undergo drastic transformation via small-scale ocean turbulence, as revealed by the significant change in temperature values before/after the Samoan Passage. Measurements of the flow through the main channel **b** show elevated turbulent mixing at two sills (**c**, black profiles) with the coldest deep water completely mixed away (**c**, color). Highly resolved towed measurements at the second sill show details of turbulent mixing (**d**, color), and internal waves are visible in the temperature contours (**d**, black lines). Adapted from Alford et al. (2013)[23].

waters of the deep Pacific. Detailed sampling of the temperature structure (Fig. 2c) and turbulent mixing (assessed from the dissipation of turbulent kinetic energy sampled by microstructure probes; Fig. 2d) reveals steep isotherms associated with the breaking of gigantic (200-300 m high) internal waves. Such wave roll-ups and their breaking initiate a turbulent energy cascade towards smaller scales, which unfolds until energy reaches the limit where molecular processes become of leading order. Hence, turbulence leads to the dynamics described by Lewis Fry Richardson's famous quote "big whirls have little whirls that feed on their velocity, and little whirls have lesser whirls and so on to viscosity", and illustrated in the inset in Fig. 1. Through the formation of whirls and filaments, turbulence accelerates molecular diffusion. As a result, momentum, heat, salt, and passive tracers, such as carbon and nutrients are irreversibly mixed (homogenized) across the stable density stratification[22]. In the Samoan Passage example, this microscale physics causes the dense (colder) bottom waters to mix with lighter (warmer) overlying waters, homogenizing the temperature gradient (Fig. 2c) and leading to net upwelling of the cold waters[23]. In practice, it is difficult to measure the big and small whirls at the same time and, often, information is only available on one narrow set of scales, thus necessitating assumptions about the existence of a (forward, namely towards smaller scales) turbulent cascade, following Kolmogorov's seminal K41 theory[24], even though stratified turbulence is demonstrably, inherently anisotropic and inhomogeneous.

In most applications, we are concerned with the turbulent flux of a scalar tracer, as this turbulent flux leads inevitably to irreversible mixing. Taking the turbulent flux of buoyancy as an example, and hence connecting irreversible mixing directly to exchanges between the kinetic energy and potential energy reservoir[14], mixing may be expressed via

$$\mathcal{M} = \overline{w'b'} \approx -\Gamma\varepsilon \approx -\kappa\partial_z b \approx -\frac{\chi\partial_z b}{2\theta_z^2}, \qquad (1)$$

where $b = -g(\rho - \rho_0)/\rho$ is buoyancy (with g, ρ, and ρ_0 being the gravitational acceleration, density, and reference density, respectively), and the turbulent flux is given by the covariance of fluctuations in diapycnal velocity (w') and buoyancy (b'). κ is the effective diapycnal ($\sim$ vertical) diffusivity. Assuming that density is mostly determined by temperature (θ in Eq. (1) is potential temperature), the flux may be approximated by inferring κ from estimates of χ, i.e., the dissipation rate of thermal variations (i.e., the rate at which temperature fluctuations are smoothed out by turbulence, and thus a fundamental measure of diffusive irreversible mixing as defined above). χ is calculated from measured temperature gradient spectra as $\chi \approx 2D_\theta < \nabla\theta^2 >$, where D_θ is thermal diffusivity. Alternatively, a classical assumption is to assume that the turbulent flux can be approximated by $\Gamma\varepsilon$, where ε is the rate of turbulent kinetic energy dissipation[25] and Γ is the flux coefficient. The flux coefficient is computed as the ratio of the power available for mixing to viscous dissipation rate of turbulent kinetic energy. Notably, ε can be assessed from observations, whereas the flux is notoriously difficult to measure directly[22,26]. Thus, Γ connects the 'observable' ε to the 'desired' $\mathcal{M}$. As such, its parameterization based on observable quantities has been the subject of intense research (and controversy) over the past four decades[12,14,27–30].

Although a constant value of $\Gamma = 0.2$ is still commonly adopted in practice, its variability and dependency on the nature of turbulence are well appreciated[14,30,31]. In particular, there is clear evidence that it depends on (at least) three different non-dimensional parameters capturing different aspects of the flow properties[32]. First, there is long-standing numerical evidence[33,34] that Γ is a decreasing function of the molecular Prandtl number $Pr = \nu_m/\kappa_m$, (where ν_m and κ_m are the molecular values of the kinematic viscosity and the density diffusivity respectively) which appears to be related to the possibility of the development of fine-scale 'ramp-cliff' structure in the buoyancy field for flows with higher values of Pr[35]. Second, the dependence of the properties of stratified turbulence on the 'intensity' or buoyancy Reynolds number $\varepsilon/(\nu\partial_z b)$ has long been postulated[36,37]. There is strong numerical[31,38] and observational evidence[39] that (at least in some circumstances) Γ varies like $Re_B^{-1/2}$ for sufficiently large Re_B, although this is still a topic of ongoing discussion. Indeed, demonstrating just how challenging modeling stratified turbulent mixing is, highly plausible theoretical arguments have been advanced that Γ should depend fundamentally on a third parameter, the turbulent Froude number $Fr = \varepsilon/(\mathcal{K}\partial_z b)$, where $\mathcal{K}$ is the turbulent kinetic energy[40–42]. These arguments are supported by observational[33,43,44] and numerical evidence[41,42], and there is some (though not yet conclusive) evidence that apparent variation with Re_B may actually be associated with a correlated variation with Fr[45]. Such variability of mixing with various parameters has been shown to have non-negligible impacts on the net mixing-driven circulation, and should therefore be taken into account when parameterizing turbulence in ocean models[31,46,47], although it is (at the moment) not at all settled how such variability should robustly and credibly be parameterized.

Observing mixing

Assuming turbulence to be isotropic, turbulent fluxes can be inferred from estimates of ε or χ, following Eq. (1)[48]. Ship-deployed microstructure profiler measurements define the gold standard in the direct observational inference of mixing in the ocean interior. These profilers return velocity shear and thermal variance observations, from which ε and χ can be inferred, respectively. Such observations are scarce due to their technical difficulty and cost[49], and coincident observations of large-scale flow and turbulent mixing (such as the study in Fig. 2) are rarely available. Indirect inferences of turbulence may also be made from temperature and salinity, regularly sampled through global international ship-based programs, such as WOCE, GO-SHIP and GEOTRACES, or the global profiling float array deployed by the Argo Program[50–56]. Such indirect inferences, made based on the 'finestructure' in thermohaline and velocity variables, have proven successful in identifying areas of elevated turbulence in the ocean interior[57,58], but can be inaccurate by as much as one order of magnitude due to diverse assumptions and uncertainties[59]. Finally, dye and tracer release experiments have been successfully used to provide direct measures of mixing[26,60,61]. These release experiments measure the bulk spatio-temporal mixing that water parcels experience, thereby allowing us to quantify the net effect of mixing on tracer distributions. This makes it possible to constrain turbulence parameterizations in ESMs, although linking these estimates to individual turbulent processes or spatio-temporal distributions of mixing rates is challenging[62].

Modeling mixing

In ESMs, mixing is parameterized with turbulent diffusivity, κ, which expresses the unresolved subgrid-scale mixing in terms of resolved, coarse-grained density gradients (Eq. (1)). Despite decades of research, the representation of κ in the ocean interior remains poor regardless of model resolution[63,64], and is often dominated by numerical effects (so-called "spurious" or "numerical mixing")[65,66]. Even high-resolution, internal wave-permitting regional models cannot fully resolve turbulent processes and must employ parameterizations for turbulent diffusion of density, momentum and tracers. Commonly adopted parameterizations of the turbulent diapycnal diffusivity, such as the K-Profile parameterization (KPP)[67], do not permit coupling of the density and momentum budgets[68]. As a result, in all existing ESMs, no energetic link exists between resolved/permitted processes that can contribute to mixing and the actual mixing in the models. Our best representation of mixing in ESMs is based on prescribed estimates of energy transfer from the larger-scale flow to small-scale turbulence[15,69–71], combined with Eq. (1). Using this approach, ESMs incorporate sensitivities to parameterizations of internal tides[47,72–74], wind-driven near-inertial waves[75], lee waves[15,72,76], and boundary layer turbulence[77]. While the contributions associated with these processes are often added up linearly in ESMs, in reality, such processes often coexist and undergo nonlinear interactions. Further, the energy transfer from large to small scales is neither a function of the state of the model (i.e. one-way feedback), nor is unconnected to the model's energy budget. Thus, the lack of critical energetic connections in coarse-resolution IPCC-class ESMs compromises the models' ability to simulate the climatic variability induced by variations in ocean mixing.

Climatic reach of small-scale ocean turbulence

Small-scale turbulence in the ocean interior exerts a leading-order climatic influence on timescales ranging from millennial to sub-annual, and on spatial scales ranging from thousands of kilometers to meters. Turbulent mixing in the ocean interior exerts a modulation on the climate through a variety of multi-scale mechanisms—by modifying water mass properties, altering oceanic heat content, regulating biogeochemical processes and oceanic carbon storage, and impacting climatic feedbacks (Fig. 3). Most of these processes lack a physically credible representation in ESMs. Per each process, the red-to-green circle color indicates whether there has been little or no attempt to represent such process in even the most advanced climate models (red); some attempt has been made, but the representation is most likely inadequate on climate-relevant timescales of seasons to decades/centuries (yellow); or some attempt has been made, and the representation is potentially adequate (green).

Here, we select a subset of these processes to illustrate how small-scale turbulence in the ocean interior contributes to modulating climate variability on a wide span of spatio-temporal scales, and through processes largely absent from climate models. This articulates the need for substantial improvements in mixing parameterizations.

Mixing and the global ocean circulation and stratification

Dense waters formed at high latitudes in the northern North Atlantic and around Antarctica fill up the deep and abyssal ocean and constitute the main component of the global-scale Meridional Overturning Circulation (MOC; Fig. 1). By connecting water masses across the full depth of the ocean, the MOC induces a large-scale redistribution of heat, carbon and nutrients that is key to the Earth's climate and biogeochemical cycles[78] (Fig. 1). Turbulent mixing sustains the MOC by providing energy to overcome the stable stratification, and so to upwell deep waters back to shallower layers[2,79]. Without such dense-to-light water mass transformation, the abyssal ocean would slowly become a pool of cold, stagnant water[80]. In other words, ocean turbulence is critical to establishing and maintaining deep-ocean stratification, thereby contributing to the equilibration of deep circulation on centennial and longer timescales.

However, such net deep-water upwelling has a nontrivial spatio-temporal structure, and is the residual of larger upwelling and downwelling regions[31,47,81–84]. The dipolar patterns of upwelling/downwelling around topographic features result from the transition from weaker mixing in the ocean interior to enhanced boundary turbulence as one approaches the rough seafloor[46,83]. The diapycnal velocity, w, represents the local turbulence-induced dense-to-light (upwelling) and light-to-dense (downwelling) water mass transformation. In the deep ocean, on a density surface with an average depth of 3000 m, there is predominant upwelling along seafloor boundaries, and downwelling in the ocean interior (Fig. 4a; inset shows the details of the opposing up/downwelling pattern around a boundary, with upwelling limited to the boundary proximity). The diapycnal velocity is calculated here as $w = \partial_z \mathcal{M} / \partial_z b$, where $\mathcal{M}$ is inferred from Eq. (1) using recent estimates of the global distribution of tidally-induced mixing[70], $\partial_z b$ is evaluated from hydrographic data[50], and the conventional assumption $\Gamma = 0.2$ is adopted[47,70]. Variations in Γ[85] (for example with the various non-dimensional parameters discussed above) significantly alter the upwelling/downwelling patterns, with changes of the same order of magnitude as w (Fig. 4b). Such changes have potentially significant implications for inter- and cross-basin water mass exchanges. A variable Γ might have high values in zones of very weak mixing away from ocean boundaries, intermediate values ($\Gamma = 1.3\text{-}1.7 \times 0.2$) that lead to 'optimally' mixing patches close to rough topography[44,85], and $\Gamma = 0$ at the seafloor (no normal flux boundary condition). Note that, since Γ essentially describes the energy fractionation between the rates of turbulent mixing and dissipation, it has different meanings when applied to a single turbulence event or a coarse grid cell (such as the 0.5-degree grid on which calculations in Fig. 4 were performed). The latter is a bulk property, referred to as Γ_B in the figure, accounting for the cumulative statistics of the many turbulent events that occur within the volume of such a grid cell[85].

https://doi.org/10.1038/s41467-026-73809-3

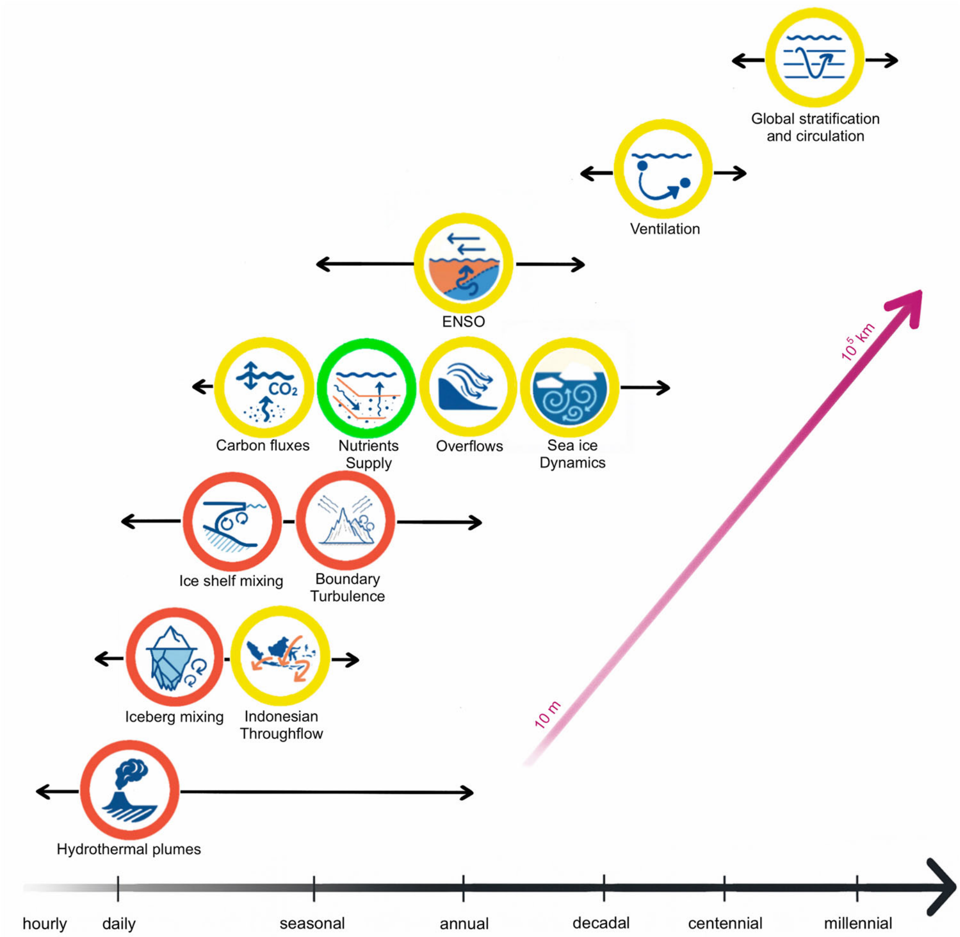

Fig. 3 | Climatic reach of small-scale turbulence in the ocean interior. A non-exhaustive overview of processes of climate significance implicating turbulent mixing, including: the dispersal of nutrient-rich hydrothermal plumes[136–138]; the vertical exchange of heat and nutrients following glacier and iceberg calving[139,140]; tidally-driven cooling of surface waters in the Indonesian Throughflow, with impacts on air-sea heat fluxes, atmospheric drying and precipitation[141,142]; the ocean-driven melting of ice shelves and mixing-modulated offshore transport of meltwater plumes[143–145]; the turbulent transformation of water masses and exchange of properties near and above the (rough) seafloor[112,146]; the mixing-regulated air-sea carbon fluxes and primary productivity in the Southern Ocean[102,147]; the mixing-mediated supply of nutrients and sustainance of primary productivity in subtropical gyres[98,99]; the mixing-governed modification of dense water properties in overflow plumes[148,149]; the interplay between upper-ocean mixing and sea-ice dynamics[150]; the mixing-influenced development and persistence of El Niño and La Niña phases[151]; the mixing-mediated transfer of ventilation tracers from the ocean surface to the ocean interior[152,153]; the global overturning circulation and stratification[2,80,88,154,155].

The net water mass transformation for a given density class can be inferred by globally integrating the diapycnal velocity over that density level (Fig. 4c). The opposing rates of diapycnal upwelling (red) and downwelling (blue) return a residual (net) water mass transformation (black) that is positive for the most part, indicating a net dense-to-light water mass transformation. The net transformation peaks at around 15-17 Sv (1 Sv = 10^6 m^3s^{-1}) for density class 28.1—average depth of ~3600 m—which is consistent with the amount of dense water estimated to form around Antarctica and constituting the lower limb of the MOC[79,86] (Fig. 1). This indicates that mixing in the ocean interior is indeed critical in regulating the strength of the lower MOC circulation. Variations in Γ_B can lead to up to 25–50% change in the net diapycnal upwelling, which can be translated into a 25–50% change in the strength of the abyssal MOC, given that turbulent mixing is the primary process sustaining this branch of the circulation.

Finally, we note that the diapycnal velocities and transformation rates in Fig. 4 are incomplete, as they do not account for all turbulence processes, and many such processes are not fully understood. While the generality of boundary upwelling of water masses and tracers is still an open question, recent fieldwork has shown upwelling of a dye released close to the seafloor in an energetic tidal mixing zone in a deep canyon (Fig. 4d)[26,87]. The experiment revealed a diapycnal velocity of ~100 m/day, much higher than the values shown in Fig. 4a and about 10,000 times higher than the estimated basin-mean upwelling value[88]. Similar results have been obtained through observationally constrained models in the Southern Ocean, where mixing is non-tidal and forced by eddy-topography interactions[64].

The role of mixing in global tracer budgets

While the large-scale tracer distributions are set by the equilibration timescale of the background ocean circulation, tracers can also be directly impacted by mixing on much shorter timescales. This section provides four examples, focused on the mixing of ventilation and biogeochemical tracers and of oceanic heat.

Mixing-modulated ocean ventilation in the Atlantic Ocean. Higher up in the water column, moving away from topography and thus from the mixing-dominated regime of the abyssal ocean, small-scale turbulence is generally considered a mechanism of, at best, second-order importance. This simplification is particularly true for the Atlantic Ocean, where the strength of the upper MOC limb (the clockwise (red) cell in Fig. 1) is assumed to be primarily controlled by wind-driven

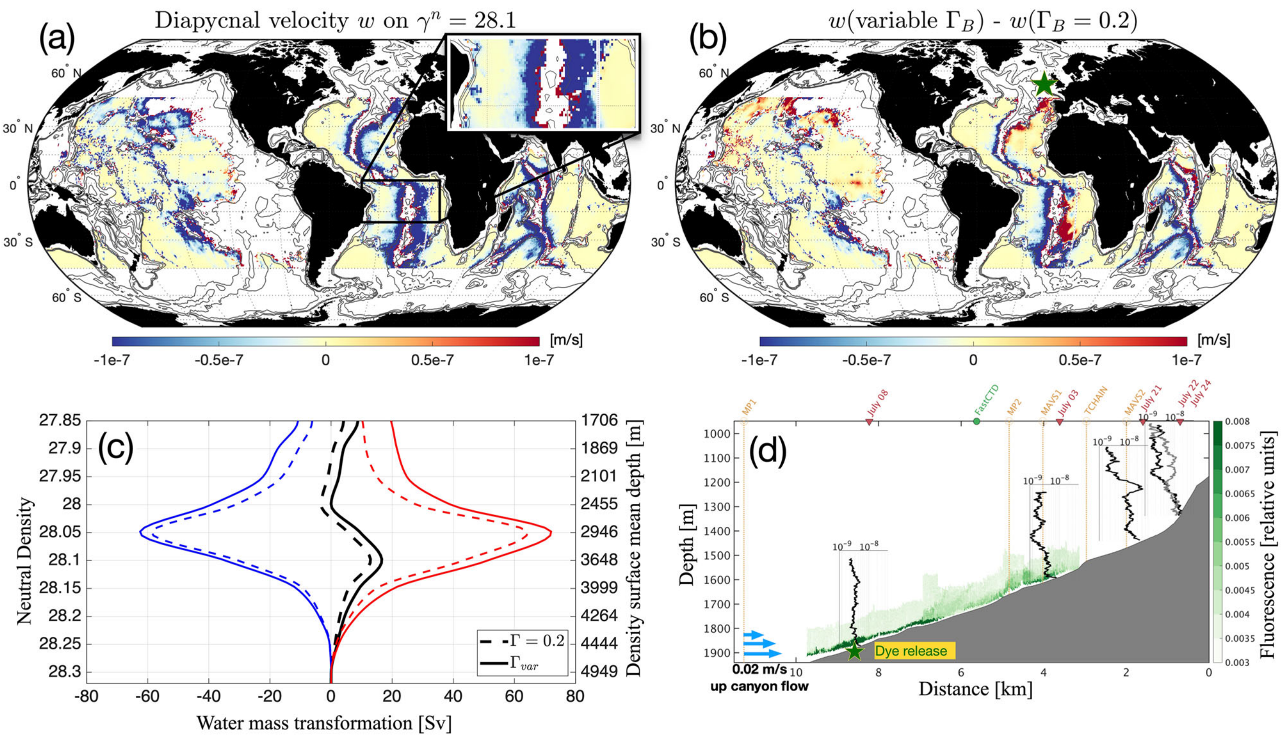

Fig. 4 | Mixing-induced upwelling near rough topography is key to abyssal ocean circulation. a Diapycnal velocity from tidally-induced mixing (estimate from de Lavergne et al., 2020[70]) on the neutral density surface 28.1 kg m^{-3} with bulk flux coefficient Γ_B = 0.2. The inset shows details of the transition from up- to downwelling in the South Atlantic. **b** Sensitivity of w to changes in the flux coefficient Γ: difference in w as calculated with a variable Γ_B, parameterized following Mashayek et al. (2022)[85], and with Γ = 0.2. **c** Global water mass transformation rates with constant and variable Γ_B, calculated by integrating the diapycnal velocity w over different density levels, spanning average depths of ~1700–4900 m. Positive (negative) water mass transformation rates indicate upwelling (downwelling). They are shown by the red and blue lines, respectively, while their residual is shown in black. Note that in (**c**) we exclude shallower depths and areas northward/southward of 45°N/S, because non-linearities in the equation of state for seawater can impact the accuracy of mixing estimates. **d** Dye concentrations after injection along a canyon in the Rockall Trough (see star in (**b**) for location). The dye concentration (fluorescence) is shown for different time steps as the dye is transported upslope by the turbulent internal tide breaking. Note that the dye is a short-term release, and hence only the upwelling part of the circulation is captured. Black lines indicate the locally observed ε. Labels denote the date of the observations and the locations of mooring stations. **a**–**c** are adapted from Cimoli et al. 2019[47] and (**d**) is adapted from Wynne-Cattanach et al. 2024[26].

upwelling of dense waters in the Southern Ocean. However, this assumption tends to obscure the effect that small-scale turbulence can have on the tracers carried by these water masses[89]. As an example, Fig. 5 shows the impact of mixing on the dispersion of transient tracers, as they are sequestered in the North Atlantic and carried southward by the upper MOC limb. Chlorofluorocarbons (CFCs) and sulfurhexafluoride (SF_6) are transient tracers that have entered the surface ocean since the 1950s, and can reveal the pathways and ventilation timescales of recently formed water masses. Ventilation timescales (i.e., water ages) can be calculated using Green's functions, which represent the local distribution of transit times from the ocean surface to an interior locale, i.e., they define the water age by representing the advection, stirring and turbulent mixing of the water parcels that start somewhere at the surface and get to a given interior location[90]. From the Green's functions, we compute the 10%, 50%, and 90% ventilation ages, defined as the times it took to ventilate 10, 50, and 90% of the water at each location (Fig. 5c)[91]. The 10% ventilation age is closer to the fastest advection timescales and is better suited to describe younger waters, whereas the 90% ventilation age corresponds to the longer equilibration timescales and is inferred by using radiocarbon observations in the deconvolution of the Green's functions[90].

The 10% ventilation age on a density surface lying at ~2000 m depth in the core of the upper MOC limb highlights the fast ventilation of the North Atlantic and the arrival of young water masses to the Southern Hemisphere, mainly via a deep western boundary current (Fig. 5a). The Green's functions at selected points along the upper MOC pathway show an apparent increase in water ages (Fig. 5). As expected, all the ventilation ages increase as we move southward, further away from the upper MOC limb source region (Fig. 5c). Beyond a longer advection timescale, the shape of the Green's functions changes significantly across the different points, with a wider distributions in the southernmost points. The increase in width indicates that the increase in age is also caused by turbulent mixing, which dilutes the transient tracer signal as it is carried southward, hence contributing to mixing the tracer-rich waters formed in the North Atlantic with the tracer-depleted ambient waters (Fig. 5c). This irreversible tracer mixing along the shown isopycnal is facilitated by stirring by mesoscale eddies[92], but it is ultimately achieved by small-scale turbulence[93,94].

Transient tracers reveal the strong mixing experienced by any tracer transported southward by the upper MOC cell (Fig. 5). This mixing can have important implications for the arrival of anthropogenic heat and carbon to the Southern Ocean via the upper MOC limb, potentially affecting air-sea carbon fluxes in the region and melt rates of Antarctic ice shelves[95,96]. As tracers are carried southward and moved diapycnally along the way (Fig. 5), they can reach the upper Southern Ocean at different locations and subsequently enter distinct pathways of the global ocean circulation, ultimately leading to very different distributions and residence times[79,89].

Turbulence-driven resupply of nutrients to the upper ocean. The combination of isopycnal and diapycnal motions resolves a long-standing conundrum of how nutrients are supplied to the euphotic

https://doi.org/10.1038/s41467-026-73809-3

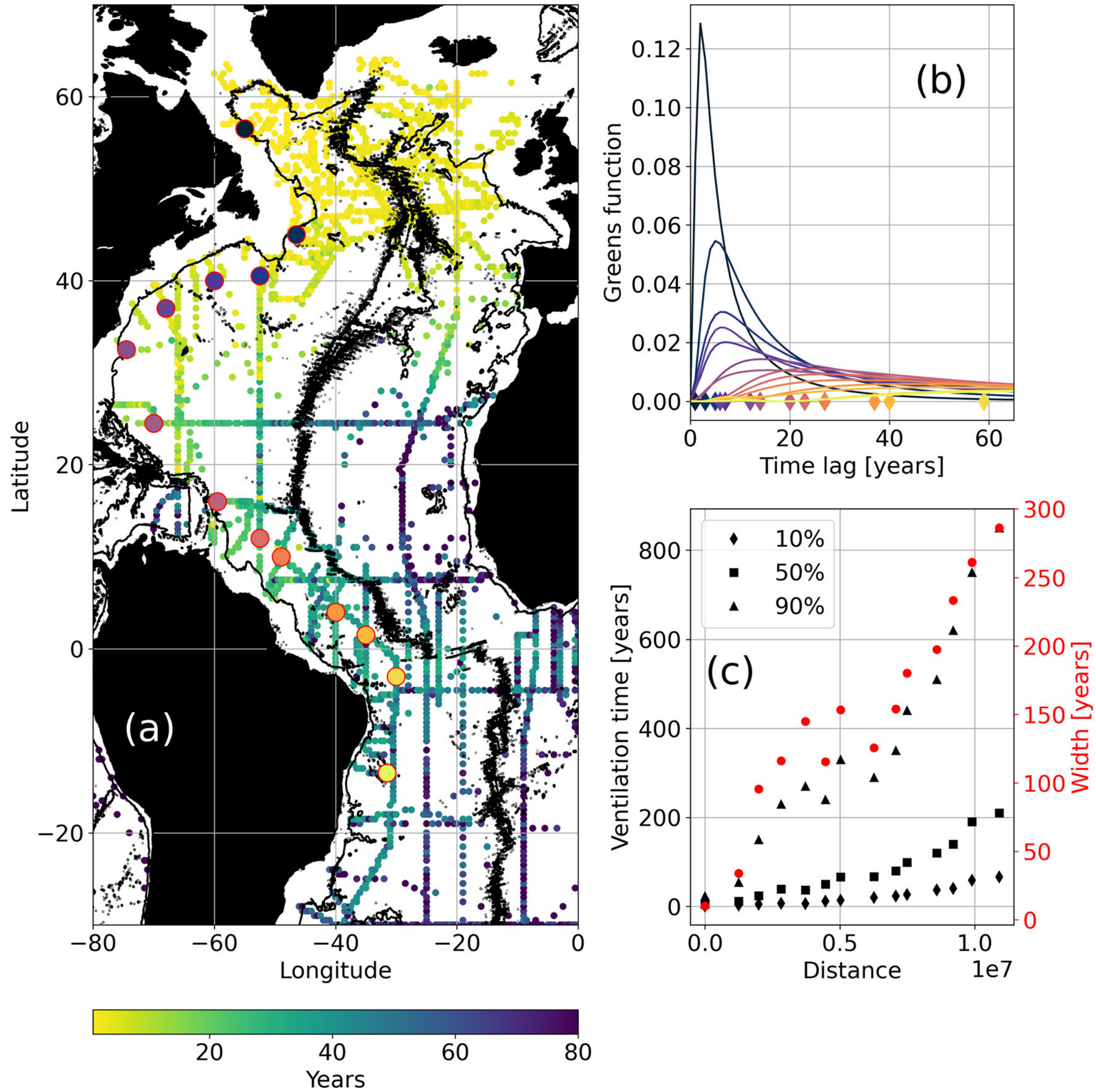

Fig. 5 | Mixing is key to sequestration and ventilation of tracers by the meridional overturning circulation. a 10% ventilation age (in years) along the neutral density surface 27.90 kg m^{-3}, which is in the core of the southward-flowing overturning branch and runs at an average depth of 2000 m in the Atlantic Ocean interior. The 10% ventilation age indicates the time taken for 10% of the water at that location to be renewed by surface-ventilated water. A few points are selected along the path of the overturning's upper limb, indicated by the circled color-coded dots. **b** Green's functions for the selected points (color-coded). The diamonds at the base of the plot indicate the 10% ventilation age for the chosen locations, which increases as we move further south away from the source of dense waters. **c** The black diamonds, squares, and triangles show the 10%, 50%, and 90% ventilation ages, respectively, for the selected points as a function of distance (in km, starting from the northernmost point in the North Atlantic). The 50% ventilation time corresponds to the median of the Green's function distribution of transit times, while 90% corresponds to the quasi-equilibrium age, usually referred to as the `mean age'. The red circles show the width of the Green's functions for the selected points as a function of distance, where the width is an indicator of the mixing experienced by the tracer while on its transit to the Southern Ocean.

zone in subtropical gyres, where the circulation is characterized by wind-driven downwelling[97–99] (Fig. 6). Nutrient supply is needed to maintain biological productivity, which regulates the amount of organic matter sequestered in the deep ocean and, hence, the net strength of the biological carbon pump, a term given to the carbon export from surface waters due to sinking organic material. About 1/3 of the total oceanic carbon sink is mediated by the biological pump. Subtropical gyres are oligotrophic regions, meaning they are usually nutrient-depleted; here, biological activity is quickly activated whenever nutrients become available. Because of their vast area, subtropical gyres can contribute a significant fraction of global carbon export (e.g., 20–50% of total North Pacific organic carbon flux) despite their low productivity[98]. Hence, a better understanding of the nutrient supply to these regions is critical to constraining the global biological carbon pump.

Recent studies have revealed that nutrients in the oligotrophic subtropical gyres are resupplied via joint contributions of along-isopycnal eddy transport (Fig. 6c) and turbulence-driven diapycnal transport (Fig. 6d)[97–99]. Diapycnal mixing transfers nutrients from thermocline waters to the euphotic zone, causing a reduction in nutrient concentration within the upper thermocline. Hence, lateral motions are needed to resupply nutrients in thermocline waters; this supply is achieved via eddy stirring, which is particularly efficient on the flanks of the gyres due to larger isopycnal slopes and lateral nutrient gradients (Fig. 6b). Ultimately, nutrient supply to the euphotic zone is achieved via a multistage (relay) mechanism that couples lateral motions with diapycnal mixing, with comparable nutrient flux convergences associated with the isopycnal and diapycnal components.

 https://doi.org/10.1038/s41467-026-73809-3

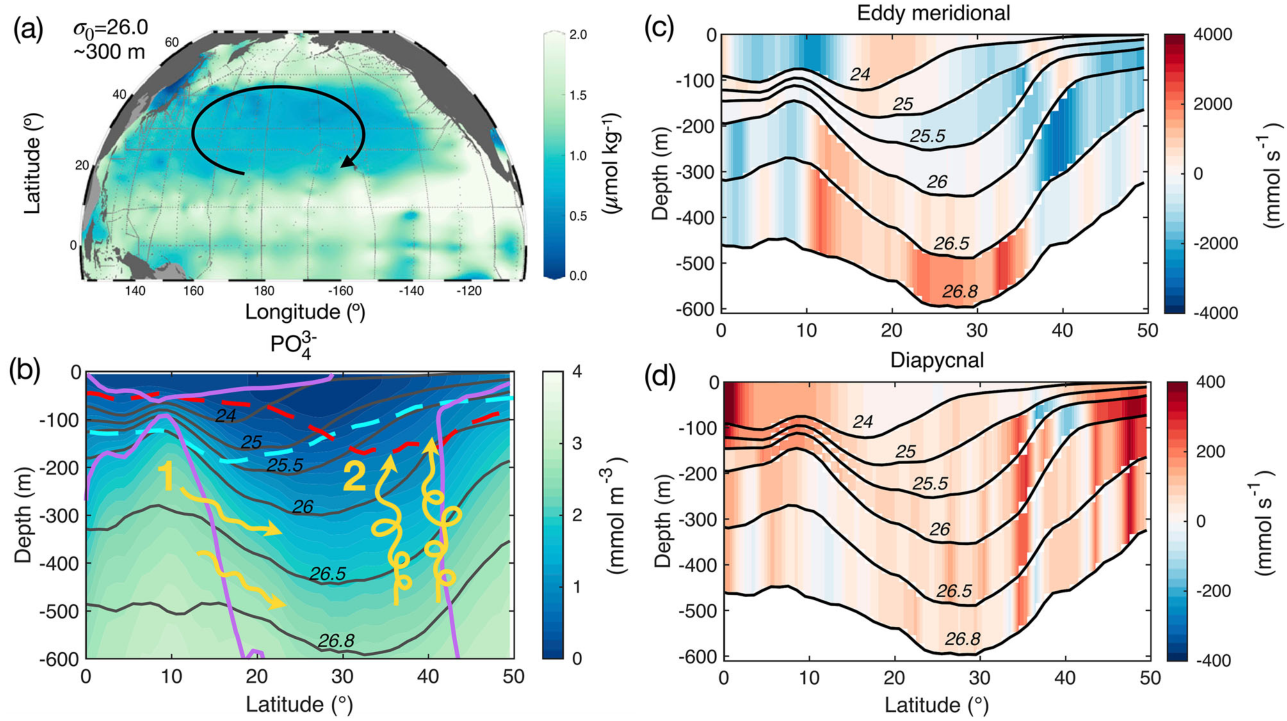

Fig. 6 | Hand-in-hand with lateral motions, vertical mixing supplies nutrients to surface biological productivity. a Phosphate (PO_4^{3-}) concentration (μmol kg^{-1}) along potential density surface σ_0 = 26.0 kg m^{-3} (approx 300 m depth) in the North Pacific basin from the Global Ocean Data Analysis Project Atlas[54]. **b** Zonal-mean phosphate concentration averaged between 1994 and 2003 over the North Pacific basin. Colored lines indicate the winter mixed layer depth (red), the summer euphotic depth (cyan), the contours of zero meridional velocity (purple), and density surfaces (black). Yellow arrows show the relay mechanisms supplying nutrients to the upper ocean through mesoscale eddy transport along density surfaces (label 1) and diapycnal mixing (label 2). **c** Basin-averaged and area-integrated meridional isopycnal eddy fluxes of phosphate (positive northward). **d** Basin-averaged and area-integrated diapycnal flux of phosphate (positive upward). Adapted from Gupta et al. (2022)[98].

Hypersensitivity of upper-ocean carbonate chemistry to mixing in the Southern Ocean. In addition to influencing the carbon budget by regulating the MOC and nutrient supply to the surface, mixing can change air-sea carbon fluxes by affecting carbon-related tracers that set the partial pressure of carbon dioxide in the ocean (pCO_2), which drives the air-sea exchange of carbon dioxide. The Southern Ocean is a region of strong carbon fluxes, where the sinking of intermediate and mode water draws carbon into the ocean interior, and the upwelling of old waters releases carbon to the atmosphere. On average, the Southern Ocean is a region of net oceanic carbon uptake, hosting nearly 40% of the ocean's anthropogenic CO_2 absorption[100,101].

Despite several decades of observations of mixing in the Southern Ocean, measurements remain sparse and difficult to scale up[102]. However, it is established that interior diapycnal mixing below the surface mixed layer is spatio-temporally variable and linked to a diverse range of dynamical processes. In ESMs, parameterized mixing primarily mimics strong turbulence along seasonal atmospheric storm tracks in the Southern Ocean, diffusing dissolved inorganic carbon (DIC) gradients over the upper few hundred meters. In other places, where strong wind-induced turbulence is lacking (such as under sea ice or ice shelves and in the ocean interior), the models rely on a prescribed background value for turbulent mixing. Elevated mixing can exist under the sea ice due to bottom-generated lee waves penetrating to the top boundary, where they can induce large vertical velocities[103], or due to shoaling of remotely generated internal tides[70], among other processes not well understood nor accounted for in models. The background mixing is typically set to a value in the range κ = 10^{-5}–10^{-4} m^2/s, with the upper bound being one or two orders of magnitude smaller than surface mixed layer turbulence induced by atmospheric forcing. Variations to the background mixing over this range change the ocean pCO_2 significantly by mixing temperature, DIC, and alkalinity (Fig. 7). This mixing effect changes the air-sea carbon dioxide flux by ~70% on annual timescales[102], highlighting the hypersensitivity of climate to the supposedly modest interior mixing.

From wind forcing to boundary turbulence: mixing-regulated deep-ocean heat content. A foremost feature of ocean climate change is the remarkably widespread warming that the deep ocean below ~2000 m has experienced since at least the 1980s[104,105]. The ocean contains ~90% of global anthropogenic warming, with approximately one third at depths below 1000 m[106]. The observed warming tracks the northward pathways of Antarctic Bottom Water (AABW), and suggests that it has been driven by processes implicated in AABW formation and/or export from source regions in the Southern Ocean.

In the South Atlantic (Fig. 8), deep-ocean warming has been shown to be controlled at least in part by wind forcing on timescales as short as days to weeks[107–109]. The forcing mechanism involves the wind-driven acceleration/deceleration of the deep western boundary current, conveying freshly produced AABW from the southern and western Weddell Sea northward into the Scotia Sea. The boundary current flows along the steep southern slope of the South Scotia Ridge (Fig. 8b), which separates the Weddell and Scotia basins, and then navigates the Orkney Passage (Fig. 8a), a deep cleft in the ridge that channels a substantial fraction (up to one quarter) of all AABW exported from the Southern Ocean[110,111]. As the boundary current experiences topographic drag, a downslope Ekman flow ensues at the current's base that advects relatively light waters under denser waters near the seabed, tilting isopycnals toward the vertical and enhancing lateral density and velocity gradients there (Fig. 8d). Such boundary-focused modification of physical gradients creates the conditions necessary for the generation of submesoscale instabilities[112]. These instabilities give rise to turbulent overturning motions, which

 https://doi.org/10.1038/s41467-026-73809-3

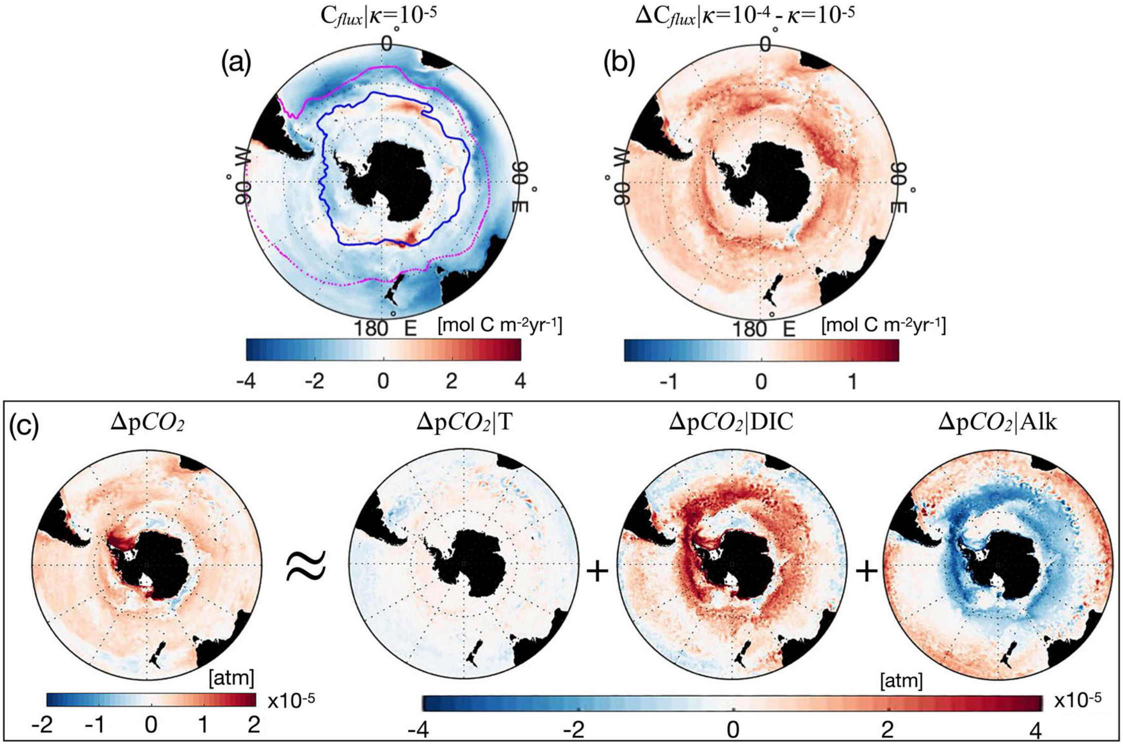

Fig. 7 | Tracer mixing below the mixed layer can impact air-sea fluxes significantly and rapidly. a Annual-mean air-sea carbon flux when background diapycnal diffusivity is set to 10^{-5} m^2/s. Negative (positive) flux indicates a net oceanic carbon sink (outgas). **b** Change in the air-sea carbon flux due to enhancement of background diffusivity to 10^{-4} m^2/s. Positive values imply reduced carbon uptake or increased outgassing. **c** Change in partial pressure of CO_2 (pCO_2) of seawater explained as contributions from the enhanced mixing-induced changes to temperature, dissolved inorganic carbon (DIC), and alkalinity (Alk); the difference between atmospheric and oceanic pCO_2 levels drives the air-sea carbon flux. Adapted from Ellison et al. (2022)[102], and based on an observationally constrained model.

vigorously mix the denser classes of AABW with overlying warmer waters (Fig. 8c), thus transferring heat into—and warming—the AABW. This heat transfer induces diapycnal upwelling of AABW near topography and diapycnal downwelling of waters above[113] (Fig. 8e).

In summary, as a result of the above mixing-mediated dynamics, stronger (weaker) eastward winds over the northern Weddell Sea induce rapid warming (cooling) of the AABW exported from the Weddell Sea[109]. This mechanism contributes significantly towards explaining the interannual variability in AABW volume and deep-ocean heat content of the Scotia basin[107,114].

Future outlook

In this perspective, we have illustrated how small-scale turbulent mixing in the ocean interior shapes the ocean's role in the climate system on sub-annual to millennial timescales, by outlining a non-exhaustive set of case examples. Thanks to regional and global observational programs, and advances in dynamical theory and high-performance computing, our phenomenological understanding of mixing and its larger-scale impacts has evolved rapidly over the past decade. Nevertheless, significant obstacles remain to fully unravel the key mechanisms and climatic impacts of small-scale turbulence in the ocean interior. Below, we discuss such obstacles and offer perspectives on where and how targeted resources could be deployed to accelerate progress.

Physics and statistics of turbulence

Recent research on the fluid dynamics of shear-driven turbulent mixing has established that the temporal evolution of a mixing event must be accounted for and, if possible, modeled. In other words, 'history matters' in mixing, due to the long-lasting imprint of larger-scale stirring onto the irreversible, small-scale turbulence. Hence, caution must be taken in interpreting data constructed from snapshots at different stages in the flow evolution[32]. Furthermore, particular care must be exercised when parameterizing mixing in terms of 'local' (in space and time) values of parameters, such as Re_B and/or Fr as defined above, as such an Eulerian approach will inevitably miss the clearly important Lagrangian effects on the mixing of the various fluid elements' history. Of course, just as assuming Γ takes a constant value is a natural first modeling step, clearly 'useful' even though obviously 'wrong', so too developing parametric models for variable Γ promises to lead to enhanced insight and predictive power in larger-scale global climate models.

However, deterministic dynamics-based models can only go so far. Understanding and modeling the inherently statistical characteristics of small-scale turbulence, with the specific aim of connecting turbulence phenomenology to large-scale budgets relevant to operational climate modeling, is perhaps the largest remaining challenge. This scale issue is further complicated by our incomplete understanding of non-linear eddy-wake interactions, e.g., the dynamics of internal tides interacting with fronts/eddies or of waves trapped in the bottom boundary layer. Resolving this scale issue is crucial to progress, yet arguably underdeveloped compared to our understanding of both the deterministic fluid dynamics of mixing and the role of mixing in the global circulation. It is becoming increasingly apparent that rare extreme turbulent events are disproportionally significant for the bulk mixing of a given region[9,115]. Using extensive oceanic datasets, it has been shown that ϵ is well described by a log-skew-normal distribution, where the distribution's long tail corresponds to large ϵ values, i.e., to the most energetic turbulent patches dominating the overall mixing. It is therefore necessary to develop parameterizations that allow the automatic identification of such extreme events as a path toward parameterizing appropriate bulk mixing statistics, for

 https://doi.org/10.1038/s41467-026-73809-3

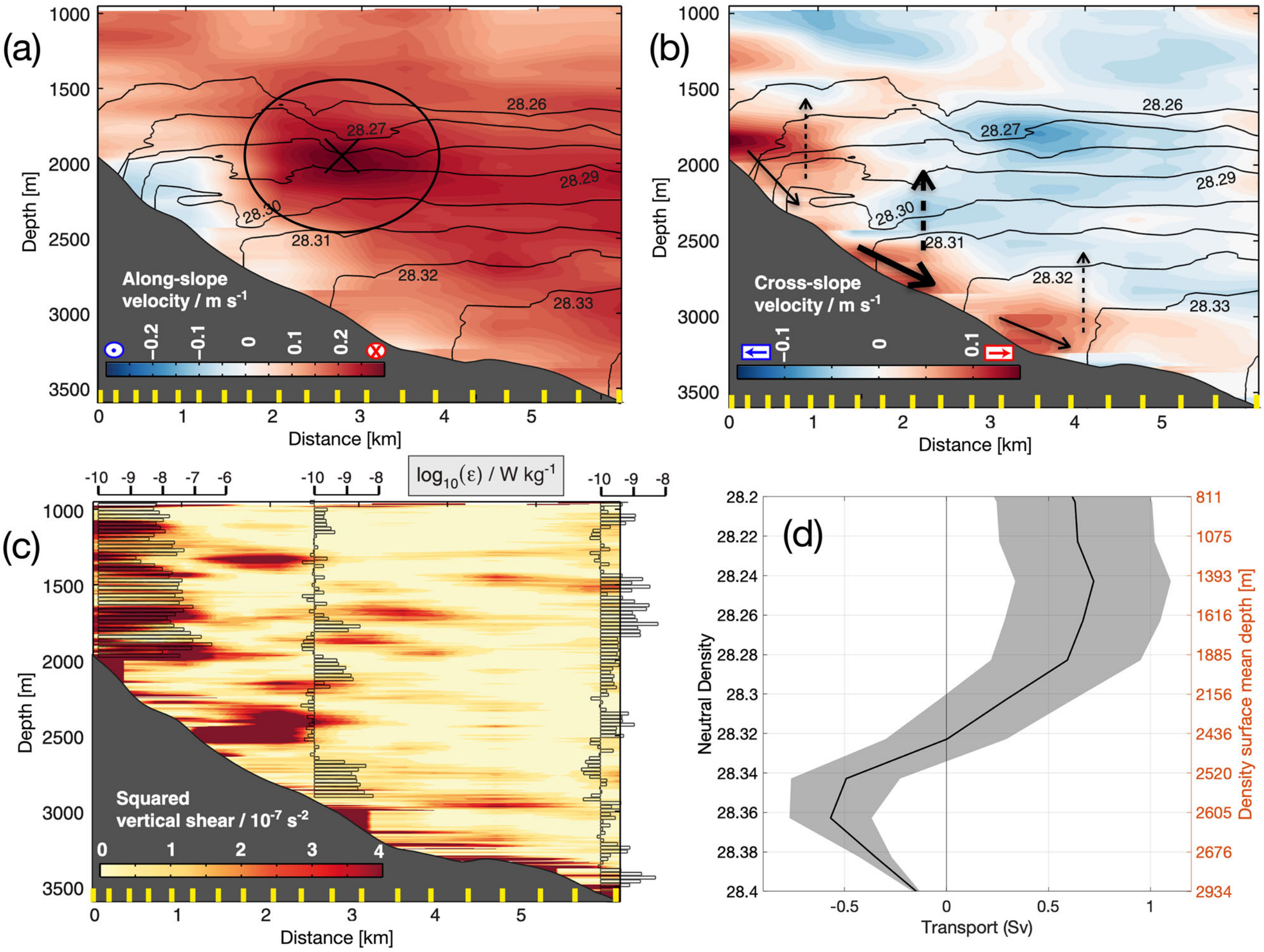

Fig. 8 | Mixing regulates deep ocean heat content. a Major Antarctic Bottom Water (AABW) pathways (yellow) in the South Atlantic. **b**–**d** show observations collected in the Orkney Passage region, indicated by the red rectangle in (**a**). **b**–**d** Fine-resolution transect across the abyssal boundary current near the Orkney Passage sill. **b** Along-slope velocity (color, with flow direction, indicated above the color bar and by the schematic) and neutral density (black contours). **c** Squared vertical shear (color), and rate of turbulent kinetic energy dissipation (ε, shaded bars). **d** Cross-slope velocity (color) and neutral density (black contours). The arrows show a schematic of the downslope Ekman flow (solid) and diapycnal mixing (dashed), with thicker lines indicating stronger transports. **e** Diapycnal transport within the deep passage, where positive values indicate water moving toward lighter classes. Adapted from Naveira Garabato et al. (2019)[112] and Spingys et al. (2021)[113].

example, via a variable flux coefficient. Any variations in the flux coefficient Γ are currently absent from ESMs, and we have argued here that their global importance needs to be examined (Fig. 4). New studies of the statistical characteristics of small-scale turbulence may steer the design of novel ESM-purposed parameterizations and, crucially, point to a significant future role for applications of machine learning to this problem[9,44,85]. Such efforts can also guide the closure of the gap between bulk measures of mixing as inferred from tracer-release experiments, and the in situ observations of turbulence, a discrepancy often linked to a historical discussion on 'missing mixing' within the ocean mixing community[61,62,116,117].

Observations

Over the past five decades, since the classical work of Walter Munk[88], significant observational efforts have been dedicated to the quantification of mixing in the ocean interior[4]. Now, small-scale turbulent fluxes have been added to the list of observable Essential Ocean Variables[22], given their recognized climatic reach on a number of spatial and temporal scales. The last few decades have seen huge technological advancements in mixing observations, but greater impetus is needed to reach global coverage and gain critical insight into the statistics of small-scale turbulent mixing.

In recent years, advances in mobile electronics have led to the development of low-power turbulence sensors[118], and there are ongoing efforts to add such turbulence probes to global autonomous observational systems, such as the Argo program[119]—which would enormously expand observational coverage. However, more wide-reaching turbulence-measuring technologies are required, especially near boundaries (including the climate-critical sea ice-ocean and ice shelf-ocean boundaries[120–122]) and in the deep ocean, where direct measurement of turbulent fluxes is technically most challenging and currently out of reach of core Argo floats. Technological advances have made velocity-sensing techniques (such as travel-time velocimetry and particle tracking velocimetry) feasible and inexpensive for mounting on moorings and turbulence platforms[123]. These new sensing techniques can return time series of the turbulent buoyancy flux (i.e., direct mixing observations), as well as of turbulent kinetic energy dissipation. Similarly, distributed sensing along fiber optic cables (regularly deployed for energy and communication purposes) provides a new approach to making oceanographic measurements at a very large spatio-temporal scale (10 cm, 1 kHz) and sustained over long periods. These approaches have shown early promise to afford a new window on turbulent processes[124]. Such observations could provide a transformative high-resolution view of ocean turbulence near the seafloor (for a seabed cable) or along a vertical profile (for mooring deployments). All these novel technologies can supply information to constrain the characteristics and statistics of small-scale turbulent mixing thoroughly[42,44]. As the statistics of mixing become increasingly better-resolved by observations, the representation of mixing in high-resolution numerical simulations can be tested, narrowing the gap between modeling and observational efforts.

Finally, we have shown that mixing acts differently on distinct tracers. While the impact of mixing on the ocean interior's density stratification can manifest in climatic trends (through the mixing-circulation two-way feedback) on centennial to millennial timescales, its impact on nutrient transport, primary productivity, and air-sea carbon fluxes can occur on timescales as short as sub-annual (Fig. 3). Measuring biogeochemical cycling indicators alongside mixing processes by integrating biological- and physical-oceanographic field campaigns will be helpful for improving our understanding of how mixing shapes marine biogeochemical cycles.

Modeling

We have provided evidence of the leading-order impacts of mixing on important physical and biogeochemical processes, with implications for the modulation of climate variability. To capture such feedbacks in ESMs, several improvements are necessary.

Currently, ESM representations of mixing lack the ability to capture the two-way feedback between changes to mixing and changes in the climate system, as they do not have the freedom to mix less where there is less to mix, or mix more where there is more to mix, and energy is available for it. In other words, an energetically sound coupling between the momentum and density budgets is required, but is entirely lacking at present. An adaptive mixing scheme—one which would be zero in an unstratified region and also zero in a sufficiently strongly stratified region—allows for internal variability that such a restoring mechanism brings about. Regardless of the subjective choices involved in parameterizing the bulk flux coefficient Γ_B, the need to implement it in ESMs is evident. We argue that enough progress has been made to explore adaptive mixing schemes in ESMs.

Moreover, the same mixing processes can yield different turbulent diffusivities (the mixing metric used by ESMs) for different tracers, depending on their time histories, distributions in the ocean interior, and local gradients. For example, different pre-industrial gradients for heat and carbon have led to oppositely signed redistributions of their anomalies over the past several centuries[125]. Thus, the representations of mixing for various tracers need to be customized, requiring tracer-specific observations and greater model parameterization flexibility.

To conclude, the small-scale mixing discussed in this article is only one (albeit arguably dominant) part of diapycnal water mass transformations in the ocean interior. The nonlinearity of seawater's equation of state gives rise to other processes, such as cabbeling, thermobaricity, and double diffusion, which are at best crudely represented in ESMs. Yet, if properly described, these processes can conceivably lead to significant transformations, especially in the upper ocean and polar regions.

AI and other data-driven approaches

Since the late 1800s, when theoretical research on the fluid dynamics of ocean turbulence began, many investigations have been devoted to understanding the physics of shear-induced turbulence. Despite all these efforts, the task of comprehending, parameterizing and modeling turbulence, through studying individual processes and their nonlinear interactions, has been outpaced by the urgency imposed by the ongoing anthropogenic climate transition for representing such processes in ESMs. Vastly enhanced computational and observational resources have yielded enormous data on various aspects of shear-driven mixing events. Exploiting the information in these data to advance the description and modeling of the underlying flows is both a challenge and an opportunity. In particular, the rapid development of data science, especially in the algorithmic development of 'artificial intelligence' (AI) and 'machine learning', is sparking a revolution in the analysis and modeling of shear-driven mixing events. Recent research combining such data-driven techniques with physics-informed models illustrates the potential for significant improvement in the skill of parameterizations compared to classical models[115,126]. Further, data-driven techniques can lead to the identification of previously unappreciated relationships between different quantities, and thereby point toward fruitful lines of attack for physics-based modeling[127]. Such an iterative connection between data-driven and physics-informed modeling promises to revolutionize the understanding of the climate system, particularly when appropriate attention is paid to the interpretability of the emergent models. These novel data-driven approaches naturally build on the seemingly coherent global statistical characteristics of small-scale turbulence highlighted herein.

Long-term climate variability

Understanding and correctly representing mixing is key to our interpretation of past marine-centered climate tipping points, and thereby to our ability to make credible predictions of potential future tipping points. In modulating the centennial-to-millennial-scale climate variability, the ocean acts as a low-pass filter of surface perturbations[128]. Small-scale mixing effectively sets the frequency of the passband. The implication is that higher-frequency variability may be observed closer to deep-water formation sites (such as the North Atlantic) but not in the far-field (e.g., in the North Pacific) because small-scale mixing has longer time to act here. This has ramifications for how we conceptualize global ocean heat and carbon uptake, and calls for revisiting the frequency content of paleo timeseries to determine the character of surface climate variations. Unraveling the effects of mixing is crucial to quantitatively connect the decadal variability inferred from modern tracer observations (e.g., CFCs, as reviewed herein) with longer-term variability recorded in the Earth System as inferred from paleo tracers[129]. An example pertains to decadal/centennial-to-millennial transients in the ocean-atmosphere system, associated with so-called 'Dansgaard-Oeschger' variability or 'Heinrich events'[130–132]. These abrupt transitions apparently involved major changes in ocean mass transports, marine biogeochemistry and oxygenation, atmospheric greenhouse gas levels, and ocean heat content. They offer a particularly useful natural laboratory for probing the potential role of small-scale turbulent mixing in rapid ocean/climate adjustments, informing the potentially looming MOC tipping points. While the dramatic changes in ocean stratification during these events must have modulated mixing significantly, the extent to which these modulations fed back into climate variability remains poorly understood, compromising our interpretation of paleo-proxy records. Thus, ocean mixing lies at the heart of the much-needed but largely lacking effort to quantitatively link the paleo record to computational (and increasingly AI-driven) modeling of modern and future climate change.

References

1. Williams, R. & Follows, M. *Ocean Dynamics and the Carbon Cycle* (Cambridge University Press, 2011).
2. Wunsch, C. & Ferrari, R. Vertical mixing, energy, and the general circulation of the oceans. *Annu. Rev. Fluid Mech.* **36**, 281–314 (2004).
3. Talley, L. D. et al. Changes in ocean heat, carbon content, and ventilation: a review of the first decade of GO-SHIP global repeat hydrography. *Annu. Rev. Mar. Sci.* **8**, 185–215 (2016).
4. Whalen, C. B. et al. Internal wave-driven mixing: governing processes and consequences for climate. *Nat. Rev. Earth Environ.* **1**, 606–621 (2020).
5. Garabato, A. C. N. & Meredith, M. Ocean mixing: oceanography at a watershed. In *Ocean Mixing*, 1–4 (Elsevier, 2022).

6. Baker, M. A. & Gibson, C. H. Sampling turbulence in the stratified ocean: Statistical consequences of strong intermittency. *J. Phys. Oceanogr.* **17**, 1817–1836 (1987).
7. Gibson, C. H. Fossil turbulence and intermittency in sampling oceanic mixing processes. *J. Geophys. Res.: Oceans* **92**, 5383–5404 (1987).
8. Gregg, M. C., Seim, H. E. & Percival, D. B. Statistics of shear and turbulent dissipation profiles in random internal wave fields. *J. Phys. Oceanogr.* **23**, 1777–1799 (1993).
9. Cael, B. & Mashayek, A. Log-skew-normality of ocean turbulence. *Phys. Rev. Lett.* **126**, 224502 (2021).
10. Morrison, H. et al. Confronting the challenge of modeling cloud and precipitation microphysics. *J. Adv. Model. Earth Syst.* **12**, e2019MS001689 (2020).
11. Winters, K., Lombard, P., Riley, J. & D'Asaro, E. A. Available potential energy and mixing in density-stratified fluids. *J. Fluid Mech.* **289**, 115–128 (1995).
12. Ivey, G. N., Winters, K. B. & Koseff, J. R. Density stratification, turbulence, but how much mixing? *Annu. Rev. Fluid Mech.* **40**, 169–184 (2008).
13. Tailleux, R. Available potential energy and exergy in stratified fluids. *Annu. Rev. Fluid Mech.* **45**, 35–58 (2013).
14. Caulfield, C. P. Layering, instabilities, and mixing in turbulent stratified flows. *Annu. Rev. Fluid Mech.* **53**, 113–145 (2021).
15. Nikurashin, M. & Ferrari, R. Global energy conversion rate from geostrophic flows into internal lee waves in the deep ocean. *Geophys. Res. Lett.* **38**, L08610 (2011).
16. Gula, J., Molemaker, M. J. & McWilliams, J. C. Topographic generation of submesoscale centrifugal instability and energy dissipation. *Nat. Commun.* **7**, 12811 (2016).
17. Legg, S. Mixing by oceanic lee waves. *Annu. Rev. Fluid Mech.* **53**, 173–201 (2021).
18. Alford, M. H. Global calculations of local and remote near-inertial-wave dissipation. *J. Phys. Oceanogr.* **50**, 3157–3164 (2020).
19. Sarkar, S. & Scotti, A. From topographic internal gravity waves to turbulence. *Annu. Rev. Fluid Mech.* **49**, 195–220 (2017).
20. Gula, J., Taylor, J., Shcherbina, A. & Mahadevan, A. Submesoscale processes and mixing. In *Ocean Mixing* 81–214 (Elsevier, 2022).
21. Mashayek, A. et al. On the role of seamounts in upwelling deep-ocean waters through turbulent mixing. *Proc. Natl. Acad. Sci. USA* **121**, e2322163121 (2024).
22. Le Boyer, A. et al. Turbulent diapycnal fluxes as a pilot essential ocean variable. *Front. Mar. Sci.* **10**, 1241023 (2023).
23. Alford, M. H. et al. Turbulent mixing and hydraulic control of abyssal water in the Samoan Passage. *Geophys. Res. Lett.* **40**, 4668–4674 (2013).
24. Kolmogorov, A. N. The local structure of turbulence in incompressible viscous fluid for very large Reynolds numbers. *Cr Acad. Sci. URSS* **30**, 301–305 (1941).
25. Osborn, T. R. Estimates of the local rate of vertical diffusion from dissipation measurements. *J. Phys. Oceanogr.* **10**, 83–89 (1980).
26. Wynne-Cattanach, B. L. et al. Observations of diapycnal upwelling within a sloping submarine canyon. *Nature* **630**, 884–890 (2024).
27. Gregg, M. C. Diapycnal mixing in the thermocline: a review. *J. Geophys. Res. Oceans* **92**, 5249–5286 (1987).
28. Fernando, H. J. S. Turbulent mixing in stratified fluids. *Annu. Rev. Fluid Mech.* **23**, 455–493 (1991).
29. Peltier, W. R. & Caulfield, C. P. Mixing efficiency in stratified shear flows. *Annu. Rev. Fluid Mech.* **35**, 135–167 (2003).
30. Gregg, M., D'Asaro, E., Riley, J. & Kunze, E. Mixing efficiency in the ocean. *Annu. Rev. Mar. Sci.* **10**, 443–473 (2018).
31. Mashayek, A. et al. Efficiency of turbulent mixing in the abyssal ocean circulation. *Geophys. Res. Lett.* **44**, 6296–6306 (2017).
32. Caulfield, C. P. Open questions in turbulent stratified mixing: do we even know what we do not know? *Phys. Rev. Fluids* **5**, 110518 (2020).
33. Smyth, W. D., Moum, J. & Caldwell, D. The efficiency of mixing in turbulent patches: inferences from direct simulations and microstructure observations. *J. Phys. Oceanogr.* **31**, 1969–1992 (2001).
34. Salehipour, H., Peltier, W. R. & Mashayek, A. Turbulent diapycnal mixing in stratified shear flows: the influence of Prandtl number on mixing efficiency and transition at high Reynolds number. *J. Fluid Mech.* **773**, 178–223 (2015).
35. Bragg, A. D. & de Bruyn Kops, S. M. Understanding the effect of Prandtl number on momentum and scalar mixing rates in neutral and stably stratified flows using gradient dynamics. *J. Fluid Mech.* **992**, A10 (2024).
36. Gibson, C. H. Fossil turbulence, salinity, and vorticity turbulence in the ocean. In *Marine Turbulence (ed. J. C. Nihous)*, 221–257 (Elsevier, 1980).
37. Gargett, A. E., Osborn, T. R. & Nasmyth, P. W. Local isotropy and the decay of turbulence in a stratified fluid. *J. Fluid Mech.* **144**, 231–280 (1984).
38. Shih, L. H., Koseff, J. R., Ivey, G. N. & Ferziger, J. H. Parameterization of turbulent fluxes and scales using homogeneous sheared stably stratified turbulence simulations. *J. Fluid Mech.* **525**, 193–214 (2005).
39. Monismith, S. G., Koseff, J. R. & White, B. L. Mixing efficiency in the presence of stratification: when is it constant? *Geophys. Res. Lett.* **45**, 5627–5634 (2018).
40. Ivey, G. N. & Imberger, J. On the nature of turbulence in a stratified fluid. Part I: the energetics of mixing. *J. Phys. Oceanogr.* **21**, 650–658 (1991).
41. Maffioli, A., Brethouwer, G. & Lindborg, E. Mixing efficiency in stratified turbulence. *J. Fluid Mech.* **794**, 3 (2016).
42. Garanaik, A. & Venayagamoorthy, S. K. On the inference of the state of turbulence and mixing efficiency in stably stratified flows. *J. Fluid Mech.* **867**, 323–333 (2019).
43. Ijichi, T. & Hibiya, T. Observed variations in turbulent mixing efficiency in the deep ocean. *J. Phys. Oceanogr.* **48**, 1815–1830 (2018).
44. Mashayek, A., Caulfield, C. P. & Alford, M. H. Goldilocks mixing in oceanic shear-induced turbulent overturns. *J. Fluid Mech.* **928**, A1 (2021).
45. Portwood, G. D., de Bruyn Kops, S. M. & Caulfield, C. P. Implications of inertial subrange scaling for stably stratified mixing. *J. Fluid Mech.* **939**, A10 (2022).
46. de Lavergne, C., Madec, G., Le Sommer, J., Nurser, G. & Naveira-Garabato, A. The impact of a variable mixing efficiency on the abyssal overturning. *J. Phys. Oceanogr.* **46**, 663–681 (2016).
47. Cimoli, L. et al. Sensitivity of deep ocean mixing to local internal tide breaking and mixing efficiency. *Geophys. Res. Lett.* **46**, 14622–14633 (2019).
48. Thorpe, S. A. The turbulent ocean. (Cambridge University Press, 2005).
49. Shroyer, E. L., Nash, J. D., Waterhouse, A. F. & Moum, J. N. Measuring ocean turbulence. In *Observing the oceans in real time*, 99–122 (Springer, 2018).
50. Gouretski, V. World ocean circulation experiment–argo global hydrographic climatology. *Ocean Sci.* **14**, 1127–1146 (2018).
51. GO-SHIP. Global Ocean Ship-based Hydrographic Investigations Program. http://www.go-ship.org/.
52. GEOTRACERS. International Study of the Marine Biogeochemical Cycles of Trace Elements and Their Isotopes. https://www.geotraces.org/.
53. Argo Program. Argo float data and metadata from Global Data Assembly Centre. *SEANOE* https://doi.org/10.17882/42182.
54. Lauvset, S. K. et al. GLODAPv2. 2022: the latest version of the global interior ocean biogeochemical data product. *Earth Syst. Sci. Data* **14**, 5543–5572 (2022).

55. Davis, R. E. et al. 100 years of progress in ocean observing systems. *Meteorol. Monogr.* **59**, 1–3 (2019).
56. Broullón, E. et al. Isopycnal stirring and diapycnal mixing in the eastern North Atlantic inferred from Argo observations. *J. Phys. Oceanogr.* **56**, 627–641 (2026).
57. Whalen, C., Talley, L. & MacKinnon, J. Spatial and temporal variability of global ocean mixing inferred from Argo profiles. *Geophys. Res. Lett.* **39**, 053196 (2012).
58. Kunze, E. Internal-wave-driven mixing: global geography and budgets. *J. Phys. Oceanogr.* **47**, 1325–1345 (2017).
59. Polzin, K. L., Garabato, A. C. N., Huussen, T. N., Sloyan, B. M. & Waterman, S. Finescale parameterizations of turbulent dissipation. *J. Geophys. Res. Oceans* **119**, 1383–1419 (2014).
60. Ledwell, J. R., Watson, A. J. & Law, C. S. Mixing of a tracer in the pycnocline. *J. Geophys. Res.: Oceans* **103**, 21499–21529 (1998).
61. Watson, A. J. et al. Rapid cross-density ocean mixing at mid-depths in the Drake Passage measured by tracer release. *Nature* **501**, 408–411 (2013).
62. Mashayek, A. et al. Topographic enhancement of vertical turbulent mixing in the Southern Ocean. *Nat. Commun.* **8** (2017).
63. Mashayek, A., Baker, L., Cael, B. & Caulfield, C. P. A marginal stability paradigm for shear-induced diapycnal turbulent mixing in the ocean. *Geophys. Res. Lett.* **49**, e2021GL095715 (2022).
64. Baker, L., Mashayek, A. & Naveira Garabato, A. Boundary upwelling of Antarctic Bottom Water by topographic turbulence. *AGU Adv.* **4**, e2022AV000858 (2023).
65. Griffies, S. M., Pacanowski, R. C. & Hallberg, R. W. Spurious diapycnal mixing associated with advection in a z-coordinate ocean model. *Monthly Weather Rev.* **128**, 538–564 (2000).
66. Megann, A. Estimating the numerical diapycnal mixing in an eddy-permitting ocean model. *Ocean Model.* **121**, 19–33 (2018).
67. Large, W. G., McWilliams, J. C. & Doney, S. C. Oceanic vertical mixing: a review and a model with a nonlocal boundary layer parameterization. *Rev. Geophys.* **32**, 363–403 (1994).
68. Olbers, D., Eden, C., Becker, E., Pollmann, F. & Jungclaus, J. The IDEMIX model: parameterization of internal gravity waves for circulation models of ocean and atmosphere. In *Energy Transfers in Atmosphere and Ocean* 87–125 (Springer, 2019).
69. MacKinnon, J. A. et al. Climate process team on internal wave–driven ocean mixing. *Bull. Am. Meteorol. Soc.* **98**, 2429–2454 (2017).
70. de Lavergne, C. et al. A parameterization of local and remote tidal mixing. *J. Adv. Model. Earth Syst.* **12**, e2020MS002065 (2020).
71. St Laurent, L. C., Simmons, H. L. & Jayne, S. R. Estimating tidally driven mixing in the deep ocean. *Geophys. Res. Lett.* **29**, 21–1 (2002).
72. Melet, A., Hallberg, R., Legg, S. & Polzin, K. Sensitivity of the ocean state to the vertical distribution of internal-tide-driven mixing. *J. Phys. Oceanogr.* **43**, 602–615 (2013).
73. Melet, A., Legg, S. & Hallberg, R. Climatic impacts of parameterized local and remote tidal mixing. *J. Clim.* **29**, 3473–3500 (2016).
74. Tatebe, H., Tanaka, Y., Komuro, Y. & Hasumi, H. Impact of deep ocean mixing on the climatic mean state in the Southern Ocean. *Sci. Rep.* **8**, 14479 (2018).
75. Jochum, M. et al. The impact of oceanic near-inertial waves on climate. *J. Clim.* **26**, 2833–2844 (2013).
76. Trossman, D. S. et al. Impact of topographic internal lee wave drag on an eddying global ocean model. *Ocean Model.* **97**, 109–128 (2016).
77. Polzin, K. L. & McDougall, T. J. Mixing at the ocean's bottom boundary. In *Ocean mixing*, 145–180 (Elsevier, 2022).
78. Roquet, F. et al. Controls of the global overturning circulation of the ocean. *npj Clim. Atmos. Sci.* **8**, 304 (2025).
79. Talley, L. D. Closure of the Global Overturning Circulation trough the Indian, Pacific, and Southern Oceans. *Oceanography* **26**, 80–97 (2013).
80. Munk, W. & Wunsch, C. Abyssal recipes II: energetics of tidal and wind mixing. *Deep Sea Res. Part I: Oceanogr. Res. Pap.* **45**, 1977–2010 (1998).
81. Mashayek, A., Ferrari, R., Nikurashin, M. & Peltier, W. Influence of enhanced abyssal diapycnal mixing on stratification and the ocean overturning circulation. *J. Phys. Oceanogr.* **45**, 2580–2597 (2015).
82. de Lavergne, C., Madec, G., Le Sommer, J., Nurser, G. & Naveira Garabato, A. C. On the consumption of Antarctic Bottom Water in the abyssal ocean. *J. Phys. Oceanogr.* **46**, 635–661 (2016).
83. Ferrari, R., Mashayek, A., McDougall, T., Nikurashin, M. & Champin, J.-M. Turning ocean mixing upside down. *J. Phys. Oceanogr.* **46**, 2239–2261 (2016).
84. de Lavergne, C., Groeskamp, S., Zika, J. & Johnson, H. L. The role of mixing in the large-scale ocean circulation. In *Ocean Mixing* 35–63 (Elsevier, 2022).
85. Mashayek, A., Cael, B., Cimoli, L., Alford, M. & Caulfield, C. P. A physical-statistical recipe for representation of small-scale oceanic turbulent mixing in climate models. *Flow* **2**, E24 (2022).
86. Orsi, A. H., Johnson, G. C. & Bullister, J. L. Circulation, mixing, and production of Antarctic Bottom Water. *Prog. Oceanogr.* **43**, 55–109 (1999).
87. Garabato, A. C. N. et al. Connecting mixing to upwelling along the ocean's sloping boundary. *Geophys. Res. Lett.* **52**, e2025GL119186 (2025).
88. Munk, W. Abyssal recipes. *Deep-Sea Res.* **13**, 707–730 (1966).
89. Cimoli, L. et al. Significance of diapycnal mixing within the Atlantic Meridional Overturning Circulation. *Agu Adv.* **4**, e2022AV000800 (2023).
90. Cimoli, L., Gebbie, G., Purkey, S. G. & Smethie, W. M. Annually resolved propagation of CFCs and SF6 in the global ocean over eight decades. *J. Geophys. Res. Oceans* **128**, e2022JC019337 (2023).
91. Wunsch, C. & Heimbach, P. How long to oceanic tracer and proxy equilibrium? *Quat. Sci. Rev.* **27**, 637–651 (2008).
92. Sévellec, F., Kolodziejczyk, N. & Portela, E. Turbulent isopycnal mixing dominates thermohaline transformations of intermediate ocean waters. *Nat. Commun.* **16**, 9838 (2025).
93. Smith, K. S. & Ferrari, R. The production and dissipation of compensated thermohaline variance by mesoscale stirring. *J. Phys. Oceanogr.* **39**, 2477–2501 (2009).
94. Abernathey, R., Gnanadesikan, A., Pradal, M. A. & Sundermeyer, M. A. Isopycnal mixing. In *Ocean mixing*, 215–256 (Elsevier, 2022).
95. Marshall, J. et al. The ocean's role in polar climate change: Asymmetric Arctic and Antarctic responses to greenhouse gas and ozone forcing. *Philos. Trans. R. Soc. A Math. Phys. Eng. Sci.* **372**, 20130040 (2014).
96. Armour, K. C., Marshall, J., Scott, J. R., Donohoe, A. & Newsom, E. R. Southern Ocean warming delayed by circumpolar upwelling and equatorward transport. *Nat. Geosci.* **9**, 549–554 (2016).
97. Spingys, C. P. et al. Observations of nutrient supply by mesoscale eddy stirring and small-scale turbulence in the oligotrophic North Atlantic. *Glob. Biogeochem. Cycles* **35**, e2021GB007200 (2021).
98. Gupta, M. et al. A nutrient relay sustains subtropical ocean productivity. *Proc. Natl. Acad. Sci. USA* **119**, e2206504119 (2022).
99. Oglethorpe, K., Castro, B. F., Spingys, C., Naveira Garabato, A. & Williams, R. The role of mesoscale eddy stirring and microscale turbulence in sustaining biological production in the subtropical gyres. *Glob. Biogeochem. Cycles* **39**, e2024GB008180 (2025).
100. Huang, Y., Fassbender, A. J. & Bushinsky, S. M. Biogenic carbon pool production maintains the Southern Ocean carbon sink. *Proc. Natl. Acad. Sci. USA* **120**, e2217909120 (2023).

101. Dong, Y. et al. Direct observational evidence of strong CO2 uptake in the Southern Ocean. *Sci. Adv.* **10**, eadn5781 (2024).
102. Ellison, E., Mashayek, A. & Mazloff, M. The sensitivity of Southern Ocean air-sea carbon fluxes to background turbulent diapycnal mixing variability. *J. Geophys. Res. Oceans* **128**, e2023JC019756 (2023).
103. Baker, L. & Mashayek, A. Surface reflection of bottom generated oceanic lee waves. *J. Fluid Mech.* **924**, A17 (2021).
104. Purkey, S. G. & Johnson, G. C. Warming of global abyssal and deep Southern Ocean waters between the 1990s and 2000s: contributions to global heat and sea level rise budgets. *J. Clim.* **23**, 6336–6351 (2010).
105. Johnson, G. C. & Purkey, S. G. Refined estimates of global ocean deep and abyssal decadal warming trends. *Geophys. Res. Lett.* **51**, e2024GL111229 (2024).
106. Fox-Kemper, B. et al. Ocean, Cryosphere and Sea Level Change. In *Climate Change 2021: The Physical Science Basis. Contribution of Working Group I to the Sixth Assessment Report of the Intergovernmental Panel on Climate Change* (Cambridge University Press, 1211–1362 (Cambridge University Press, 2021).
107. Jullion, L., Jones, S., Garabato, A. C. N. & Meredith, M. P. Wind-controlled export of Antarctic Bottom Water from the Weddell Sea. *Geophys. Res. Lett.* **37**, 042822 (2010).
108. Meredith, M. P. et al. Synchronous intensification and warming of Antarctic Bottom Water outflow from the Weddell Gyre. *Geophysical Research Letters* **38**, 046265 (2011).
109. Auckland, C. D. et al. Wind forcing controls on Antarctic Bottom Water export from the Weddell Sea via bottom boundary layer processes. *J. Geophys. Res.: Oceans* **129**, e2024JC021089 (2024).
110. Garabato, A. C. N., Leach, H., Allen, J. T., Pollard, R. T. & Strass, V. H. Mesoscale subduction at the antarctic polar front driven by baroclinic instability. *J. Phys. Oceanogr.* **31**, 2087–2107 (2001).
111. Garabato, A. C. N., Williams, A. P. & Bacon, S. The three-dimensional overturning circulation of the Southern Ocean during the WOCE era. *Prog. Oceanogr.* **120**, 41–78 (2014).
112. Garabato, A. C. N. et al. Rapid mixing and exchange of deep-ocean waters in an abyssal boundary current. *Proc. Natl. Acad. Sci. USA* 116, 13233–13238 (2019).
113. Spingys, C. P. et al. Mixing and transformation in a deep western boundary current: a case study. *J. Phys. Oceanogr.* **51**, 1205–1222 (2021).
114. Abrahamsen, E. P. et al. Stabilization of dense Antarctic water supply to the Atlantic Ocean overturning circulation. *Nat. Clim. Change* **9**, 742–746 (2019).
115. Couchman, M. M. et al. Data-driven identification of turbulent oceanic mixing from observational microstructure data. *Geophys. Res. Lett.* **48**, e2021GL094978 (2021).
116. Ferrari, R. What goes down must come up. *Nature* **513**, 179–180 (2014).
117. Waterhouse, A. F. et al. Global patterns of diapycnal mixing from measurements of the turbulent dissipation rate. *J. Phys. Oceanogr.* **44**, 1854–1872 (2014).
118. Le Boyer, A. et al. Modular, flexible, low-cost microstructure measurements: the epsilometer. *J. Atmos. Ocean. Technol.* **38**, 657–668 (2021).
119. Roemmich, D. et al. On the future of Argo: A global, full-depth, multi-disciplinary array. *Front. Mar. Sci.* **6**, 439 (2019).
120. Holland, D. M. & Jenkins, A. Modeling thermodynamic ice–ocean interactions at the base of an ice shelf. *J. Phys. Oceanogr.* **29**, 1787–1800 (1999).
121. Kimura, S. et al. Ocean mixing beneath Pine Island glacier ice shelf, west Antarctica. *J. Geophys. Res. Oceans* **121**, 8496–8510 (2016).
122. Schulz, K., Kadko, D., Mohrholz, V., Stephens, M. & Fer, I. Winter vertical diffusion rates in the Arctic Ocean, estimated from 7Be measurements and dissipation rate profiles. *J. Geophys. Res. Oceans* **128**, e2022JC019197 (2023).
123. Polzin, K. L., Wang, B., Wang, Z., Thwaites, F. & Williams III, A. J. Moored flux and dissipation estimates from the northern deep-water Gulf of Mexico. *Fluids* **6**, 237 (2021).
124. Spingys, C. P., Garabato, A. C. N. & Belal, M. Optical fibre sensing of turbulent-frequency motions in the oceanic environment. *Sci. Rep.* **14**, 20276 (2024).
125. Williams, R. G., Katavouta, A. & Roussenov, V. Regional asymmetries in ocean heat and carbon storage due to dynamic redistribution in climate model projections. *J. Clim.* **34**, 3907–3925 (2021).
126. Mashayek, A. et al. Deep ocean learning of small scale turbulence. *Geophys. Res. Lett.* **49**, e2022GL098039 (2022).
127. Bracco, A. et al. Machine learning for the physics of climate. *Nat. Rev. Phys.* **7**, 6–20 (2025).
128. Gebbie, G. Combining modern and paleoceanographic perspectives on ocean heat uptake. *Annu. Rev. Mar. Sci.* **13**, 255–281 (2021).
129. Huybers, P. & Wunsch, C. Paleophysical oceanography with an emphasis on transport rates. *Annu. Rev. Mar. Sci.* **2**, 1–34 (2010).
130. Peltier, W. R. & Vettoretti, G. Dansgaard-Oeschger oscillations predicted in a comprehensive model of glacial climate: A “kicked” salt oscillator in the atlantic. *Geophys. Res. Lett.* **41**, 7306–7313 (2014).
131. Peltier, W. R., Ma, Y. & Chandan, D. The KPP trigger of rapid AMOC intensification in the nonlinear Dansgaard-Oeschger relaxation oscillation. *J. Geophys. Res. Oceans* **125**, e2019JC015557 (2020).
132. Menviel, L. C., Skinner, L. C., Tarasov, L. & Tzedakis, P. C. An ice–climate oscillatory framework for Dansgaard–Oeschger cycles. *Nat. Rev. Earth Environ.* **1**, 677–693 (2020).
133. Forget, G. et al. ECCO version 4: an integrated framework for non-linear inverse modeling and global ocean state estimation. *Geosci. Model Dev.* **8**, 3071–3104 (2015).
134. Stewart, A. L., Chi, X., Solodoch, A. & Hogg, A. M. High-frequency fluctuations in Antarctic Bottom Water transport driven by Southern Ocean winds. *Geophys. Res. Lett.* **48**, e2021GL094569 (2021).
135. Mashayek, A. & Peltier, W. R. Shear-induced mixing in geophysical flows: does the route to turbulence matter to its efficiency? *J. Fluid Mech.* **725**, 216–261 (2013).
136. Walter, M. et al. Rapid dispersal of a hydrothermal plume by turbulent mixing. *Deep Sea Res. Part I: Oceanogr. Res. Pap.* **57**, 931–945 (2010).
137. Saito, M. A. et al. Slow-spreading submarine ridges in the South Atlantic as a significant oceanic iron source. *Nat. Geosci.* **6**, 775–779 (2013).
138. Tagliabue, A. et al. Mechanisms driving the dispersal of hydrothermal iron from the northern mid-Atlantic ridge. *Geophys. Res. Lett.* **49**, e2022GL100615 (2022).
139. Meredith, M. P. et al. Internal tsunamigenesis and ocean mixing driven by glacier calving in antarctica. *Sci. Adv.* **8**, eadd0720 (2022).
140. Lucas, N. S. et al. Giant iceberg meltwater increases upper-ocean stratification and vertical mixing. *Nat. Geosci.* **18**, 305–312 (2025).
141. Kida, S. & Wijffels, S. The impact of the Indonesian throughflow and tidal mixing on the summertime sea surface temperature in the western Indonesian seas. *Journal of GeophysiO Res. Oceans* **117**, 305–312 (2012).
142. Steffen, J., Seo, H., Clayson, C. A., Pei, S. & Shinoda, T. Impacts of tidal mixing on diurnal and intraseasonal air-sea interactions in the Maritime Continent. *Deep Sea Res. Part II: Topical Stud. Oceanogr.* **212**, 105343 (2023).
143. Le Brocq, A. M. et al. Evidence from ice shelves for channelized meltwater flow beneath the Antarctic ice sheet. *Nat. Geosci.* **6**, 945–948 (2013).

144. Garabato, A. C. N. et al. Vigorous lateral export of the meltwater outflow from beneath an Antarctic ice shelf. *Nature* **542**, 219–222 (2017).
145. Davis, P. E. & Nicholls, K. W. Turbulence observations beneath Larsen C ice shelf, Antarctica. *J. Geophys. Res. Oceans* **124**, 5529–5550 (2019).
146. Polzin, K., Toole, J., Ledwell, J. & Schmitt, R. Spatial variability of turbulent mixing in the abyssal ocean. *Science* **276**, 93–96 (1997).
147. Ellison, E., Mazloff, M. & Mashayek, A. The rapid response of Southern Ocean biological productivity to changes in background small scale turbulence. *J. Geophys. Res. Oceans* **129**, e2024JC021158 (2024).
148. Özgökmen, T. M., Johns, W. E., Peters, H. & Matt, S. Turbulent mixing in the Red Sea outflow plume from a high-resolution nonhydrostatic model. *J. Phys. Oceanor.* **33**, 1846–1869 (2003).
149. Hirano, D., Kitade, Y., Ohshima, K. I. & Fukamachi, Y. The role of turbulent mixing in the modified shelf water overflows that produce Cape Darnley bottom water. *J. Geophys. Res. Oceans* **120**, 910–922 (2015).
150. Rippeth, T. P. & Fine, E. C. Turbulent mixing in a changing Arctic Ocean. *Oceanography* **35**, 66–75 (2022).
151. Warner, S. J. & Moum, J. N. Feedback of mixing to ENSO phase change. *Geophys. Res. Lett.* **46**, 13920–13927 (2019).
152. Waugh, D. W., Haine, T. W. & Hall, T. M. Transport times and anthropogenic carbon in the subpolar North Atlantic Ocean. *Deep Sea Res. Part I: Oceanogr. Res. Pap.* **51**, 1475–1491 (2004).
153. Shao, A. E., Mecking, S., Thompson, L. & Sonnerup, R. E. Evaluating the use of 1-D transit time distributions to infer the mean state and variability of oceanic ventilation. *J. Geophys. Res. Oceans* **121**, 6650–6670 (2016).
154. Hieronymus, M., Nilsson, J. & Nycander, J. Water mass transformation in salinity–temperature space. *J. Phys. Oceanogr.* **44**, 2547–2568 (2014).
155. Castro, B. F. et al. Global observational estimates of thermohaline transformations by interior ocean mixing. *J. Phys. Oceanogr.* **56**, 1051–1076 (2026).

Acknowledgements

LC, CPC and ES acknowledge support from Schmidt Sciences LLC for the Institute of Computing for Climate Science. LC acknowledges support from the Advanced Research and Invention Agency's BRINE project - SCOP-SE01-P09 (G130701). AM acknowledges support from UKRI-NERC (UKRI1022), US ONR (N00014-22-1-2082), and the UK Advanced Research and Invention Agency (FPCW-PR01-P015), and inspiration and support from Cleo. ACNG acknowledges U.K. Research and Innovation (UKRI) guarantee funding for a European Research Council Advanced Grant (EP/X025136/1). MHA and GV acknowledge support from National Science Foundation Ocean Sciences OCE-1029268 and OCE-1657795. LB acknowledges support from the Engineering and Physical Sciences Research Council, grant EP/X028135/1. BFC acknowledges support from the European Research Council's Consolidator Grant 101169952 (REMIX-TUNE) and the Advanced Research and Invention Agency's Forecasting Tipping Points Grant SCOP-PR01-P021 (POLEMIX). CdL has received funding from Agence Nationale de la Recherche - France 2030 as part of the PEPR TRACCS program under grant number ANR-22-EXTR-0008. GG acknowledges support from US NSF OCE-2103049. PH and HRP are supported in part by NSF AccelNet #2114717 (iDOOS), and JPL/Caltech Subcontract 80NM0018D0004-80NM0022F0019 (ECCO). JL acknowledges EPSRC doctoral training grant no. EP/T51780X/1. KO was supported by the Cambridge Climate, Life and Earth (C-CLEAR) Doctoral Training Partnership funded by the UK Natural Environment Research Council (NE/S007164/1). SGP acknowledges support from National Science Foundation Ocean Sciences NSF OCE-1850772. AS acknowledges funding from NERC (NE/V014285/1). LCS acknowledges support from NERC grant NE/V011464/1. LDT acknowledges support from National Science Foundation Ocean Sciences OCE-2023545. RGW acknowledges support from UK Natural Environment Research Council NE/W009501/1. CW was supported by the CANARI program (UKRI grant NE/W004984/1).

Author contributions

L.C., A.M., C.P.C., and A.C.N.G. conceived the idea of the paper, designed the structure, and led the writing. The remaining co-authors contributed to different sections of the paper, such as mixing definition and statistics (L.B., B.B.C., C.d.L., and W.H.P.), observing mixing (M.H.A., B.F.C., A.L.B., C.S., G.V., and B.L.W.C.), modeling mixing (L.B., J.G., P.H., H.R.P., E.S., J.R.T., and C.W.), mixing in high-latitudes (J.L., M.S., A.S., and W.H.P.), long-term climate variability (G.G., A.M.P., and L.C.S.), mixing and AI (J.L. and N.R.), and tracer budgets (E.E., G.G., K.O., S.G.P., L.D.T., and R.G.W.). All co-authors provided feedback on the whole manuscript and figures. Beyond the first four authors, the author list is in alphabetical order.

Competing interests

The Authors declare no competing interests.

Additional information

Correspondence and requests for materials should be addressed to Laura Cimoli.

Peer review information : *Nature Communications* thanks Fabien Roquet, and the other, anonymous, reviewers for their contribution to the peer review of this work.

[1]University of Cambridge, Department of Applied Mathematics and Theoretical Physics, Cambridge, UK. [2]University of Cambridge, Department of Earth Sciences, Cambridge, UK. [3]University of Southampton, Ocean and Earth Science, Southampton, UK. [4]University of California San Diego, Scripps Institution of

Oceanography, La Jolla, CA, USA. [5]University of Edinburgh, School of Mathematics and Maxwell Institute for Mathematical Sciences, Edinburgh, UK. [6]University of Chicago, Department of Geophysical Sciences, Chicago, IL, USA. [7]Sorbonne Université-CNRS-IRD-MNHN, Laboratoire LOCEAN, Paris, France. [8]Australian National University, Research School of Earth Sciences, Canberra, ACT, Australia. [9]Woods Hole Oceanographic Institution, Woods Hole, MA, USA. [10]University of Brest, CNRS, Ifremer, IRD, Laboratoire d'Océanographie Physique et Spatiale (LOPS), IUEM, Plouzané, France. [11]University of Texas at Austin, Oden Institute for Computational Engineering and Sciences, Austin, TX, USA. [12]University of Toronto, Department of Physics, Toronto, ON, Canada. [13]University of Cambridge, Department of Computer Sciences and Technology, Cambridge, UK. [14]University of Exeter, Exeter, UK. [15]National Oceanography Centre, Southampton, UK. [16]University of Liverpool, School of Environmental Sciences, Liverpool, UK. [17]National Oceanography Centre, Liverpool, UK. [18]These authors contributed equally: Laura Cimoli, Ali Mashayek. ✉e-mail: lc929@cam.ac.uk